Title

Positive Reinforcing Mechanisms between GPR120 and PPARγ Modulate Insulin Sensitivity

Journal

Cell Metabolism, 31(6)

ISSN

1550-4131

Authors

Paschoal, Vivian A

Walenta, Evelyn

Talukdar, Saswata

et al.

Publication Date

2020-06-01

DOI

10.1016/j.cmet.2020.04.020

Peer reviewed

HHS Public Access

Author manuscript

Cell Metab. Author manuscript; available in PMC 2021 June 02.

Published in final edited form as:

Cell Metab. 2020 June 02; 31(6): 1173–1188.e5. doi:10.1016/j.cmet.2020.04.020.

Positive Reinforcing Mechanisms Between GPR120 and PPARγ Modulate Insulin Sensitivity

Vivian A. Paschoal[1,2], **Evelyn Walenta**[2], **Saswata Talukdar**[2,3], **Ariane R. Pessentheiner**[2], **Olivia Osborn**[2], **Nasun Hah**[4], **Tyler J. Chi**[2], **George L. Tye**[2,5], **Aaron M. Armando**[6], **Ronald M. Evans**[4,7], **Nai-Wen Chi**[2,8], **Oswald Quehenberger**[6], **Jerrold M. Olefsky**[2,*], **Da Young Oh**[1,2,9,*]

[1]Touchstone Diabetes Center, Department of Internal Medicine, University of Texas Southwestern Medical Center, Dallas, TX 75390, USA

[2]Division of Endocrinology and Metabolism, Department of Medicine, University of California, San Diego, La Jolla, CA 92093, USA

[3]Merck & Co., Inc., SSF, 630 Gateway Boulevard, South San Francisco, CA 94080, USA

[4]Gene Expression Laboratory, Salk Institute for Biological Studies, La Jolla, CA 92037, USA

[5]Case Western Reserve University School of Medicine, 2109 Adelbert Rd, Cleveland, OH 44106, USA

[6]Department of Pharmacology, University of California, San Diego, La Jolla, CA 92093, USA

[7]Howard Hughes Medical Institute, Salk Institute for Biological Studies, La Jolla, CA 92037, USA

[8]VA San Diego Healthcare System, San Diego, California, USA

[9]Lead Contact

SUMMARY

G Protein-coupled receptor 120 (GPR120) and PPARγ agonists each have insulin sensitizing effects. But whether these two pathways functionally interact and can be leveraged together to markedly improve insulin resistance has not been explored. Here, we show that treatment with the PPARγ agonist rosiglitazone (Rosi) plus the GPR120 agonist Compound A leads to additive effects to improve glucose tolerance and insulin sensitivity, but at lower doses of Rosi, thus avoiding its known side effects. Mechanistically, we show that GPR120 is a PPARγ target gene in

*To whom correspondence should be addressed; Jerrold M. Olefsky, MD (jolefsky@health.ucsd.edu) and Da Young Oh, PhD (dayoung.oh@utsouthwestern.edu).

AUTHOR CONTRIBUTIONS

D.Y.O. conceived the project, designed the studies. D.Y.O. and V.A.P. performed most of the experiments. V.A.P. and E.W. performed hyperinsulinemic/euglycemic clamps. S.T. performed *ob/ob* mice experiments. O.O. performed RNA-seq and microarray data analysis. N.H. analyzed ChIP-seq database. A.M.A. and O.Q. performed LC/MS for eicosanoid measurement. A.R.P, T, J. C., G.L.T. assisted experiments. N.W.C. reviewed the manuscript and contributed discussions. R.M.E. contributed discussions. D.Y.O. and J.M.O analyzed, interpreted data, and co-wrote this manuscript.

DECLARATION OF INTERESTS

The authors declare no competing financial interests.

adipocytes, while GPR120 augments PPARγ activity by inducing the endogenous ligand 15d-PGJ2 and by blocking ERK-mediated inhibition of PPARγ. Further, we used macrophage-(MKO) or adipocyte-specific GPR120 KO (AKO) mice to show that GRP120 has anti-inflammatory effects via macrophages while working with PPARγ in adipocytes to increase insulin sensitivity. These results raise the prospect of a safer way to increase insulin sensitization in the clinic.

Graphical Abstract

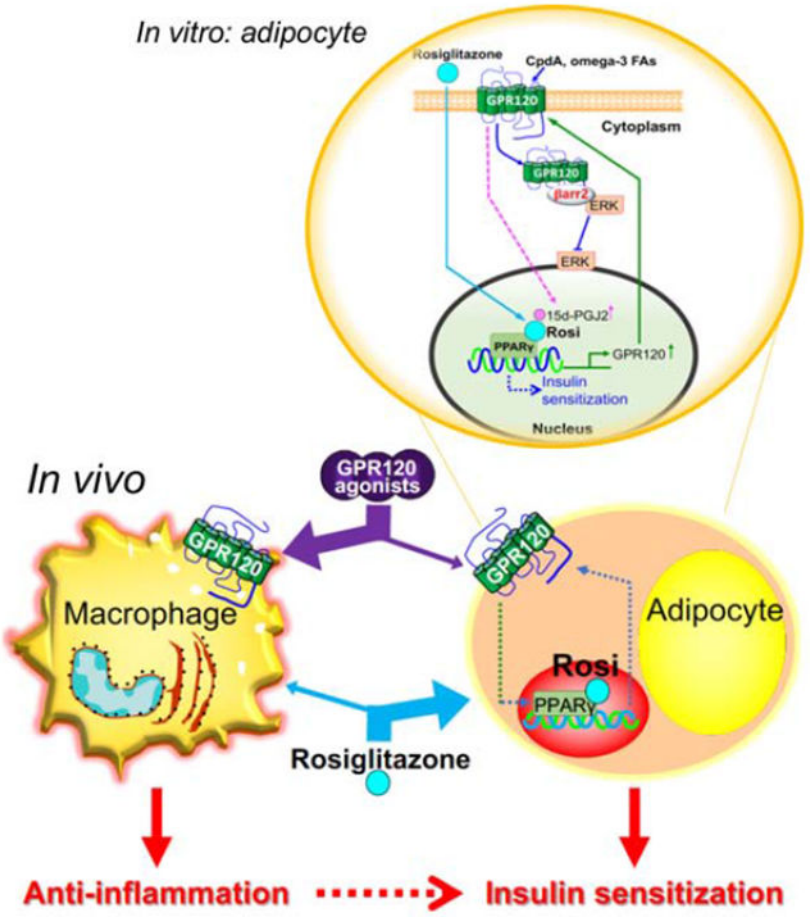

eTOC

Paschoal *et al.* explore the molecular interactions between the GPR120 and PPARγ pathways *in vitro* and *in vivo*. They also report that dual agonism of GPR120 and PPARγ additively improves insulin resistance in obese diabetic mice while avoiding the unwanted side effects of targeting PPARγ, potentially paving the way to re-expand the use PPARγ agonists in the clinic.

Keywords

GPR120; PPARγ; thiazolidinedione; Compound A; type 2 diabetes; insulin resistance; combination therapy; 15d-PGJ2

INTRODUCTION

Insulin resistance is a characteristic feature of type 2 diabetes (T2D) (Heilbronn and Campbell, 2008; Reaven, 2005; Schenk et al., 2008) and often precedes the onset of frank hyperglycemia by several years (Heilbronn and Campbell, 2008; Reaven, 2005; Schenk et al., 2008). Obesity is the dominant cause of acquired insulin resistance in man, and given the global obesity epidemic, the incidence of insulin resistance and T2D has risen sharply. While pharmacological approaches to treating T2D exist, further avenues are needed given the complex nature of the pathology. One such target may be inflammation, as obesity leads to a chronic, low-grade inflammatory state that can impair insulin sensitivity (Weisberg et al., 2003; Xu et al., 2003).

An important initiator of this chronic inflammatory response is dysfunctional adipose tissue, which plays a major role in obesity-associated insulin resistance (Tontonoz and Spiegelman, 2008). The transcription factor peroxisome proliferator-activated receptor γ (PPARγ) is critical to adipocyte differentiation (Imai et al., 2004; Tontonoz et al., 1994; Tontonoz and Spiegelman, 2008) and can modulate systemic insulin sensitivity (Tontonoz and Spiegelman, 2008). Adipocyte-specific PPARγ knockout (KO) mice develop systemic insulin resistance when fed a high-fat diet (HFD) (He et al., 2003; Medina-Gomez et al., 2007), whereas transgenic mice expressing constitutively active PPARγ in adipocytes manifest systemic insulin sensitization (Sugii et al., 2009).

Thiazolidinediones (TZDs) are high-affinity ligands for PPARγ that can improve insulin sensitivity (Lehmann et al., 1995; Tontonoz and Spiegelman, 2008; Yki-Jarvinen, 2004). One possible component of the insulin sensitizing actions of TZDs is their anti-inflammatory effects (Chinetti et al., 2000; Martin, 2010; Ricote et al., 1999). But while TZDs (notably, rosiglitazone and pioglitazone) represent current therapeutic agents for insulin resistance, their utility in the clinic for treating T2D has been limited due to adverse effects, such as edema (Basu et al., 2006; Berria et al., 2007; Nesto et al., 2004), weight gain (Fonseca, 2003; Lu et al., 2011), heart failure (Duan et al., 2005; Lago et al., 2007; Son et al., 2007) and bone loss (Bray et al., 2013; Colhoun et al., 2012).

Several reports show that G protein-coupled receptor 120 (GPR120; free fatty acid receptor 4, FFA4) activation can lead to beneficial effects in various systems (Ahn et al., 2016; Raptis et al., 2014; Wellhauser and Belsham, 2014; Williams-Bey et al., 2014; Yamada et al., 2017). Previously, we found that GPR120 is the functional receptor for omega-3 fatty acids (ω3-FAs), producing robust ω3-FA-induced anti-inflammatory, insulin sensitizing effects both *in vivo* and *in vitro* (Oh et al., 2010). In addition, the glucose intolerance and insulin resistance of GPR120 KO mice can be associated with increased glucagon secretion and enhanced hepatic glucagon sensitivity, consistent with the overall metabolic phenotype of these mice (Suckow et al., 2014). Genetic variants in the human GPR120 gene have been described in subjects with obesity and diabetes (Ichimura et al., 2012). A recent report by Quesada-Lopez *et al.* (Quesada-Lopez et al., 2016) indicated that GPR120 activation promotes brown adipose tissue (BAT) activity and browning of white fat in mice via fibroblast growth factor-21 (FGF21), suggesting that thermogenesis might be affected by GPR120. Consistent with this, GPR120 KO impaired cold-induced browning.

As the amount of exogenously administered ω3-FAs needed to adequately stimulate GPR120 to improve insulin resistance is too high to be clinically practical, small molecule GPR120 agonists have been identified for potential therapeutic use. Recently, we have shown that a high-affinity, selective GPR120 agonist (Compound A, CpdA) can reduce inflammation in macrophages *in vitro* and improve glucose tolerance and insulin sensitivity in obese mice (Oh da et al., 2014).

Given that both TZDs and GPR120 agonists can both improve insulin sensitivity, we explored the possibility that the PPARγ and GPR120 signaling pathways functionally interact. In the present study, we show that GPR120 is induced by TZD (rosiglitazone) treatment and is a direct PPARγ target gene in adipocytes. In addition, GPR120 agonism enhances PPARγ activity and stimulates the production of endogenous PPARγ ligands. Finally, *in vivo* CpdA induces potent anti-inflammatory effects in macrophages while rosiglitazone works primarily in adipocytes and these two mechanisms combine to cause additive insulin sensitization *in vivo*. The use of CpdA allows for lower, safer doses of rosiglitazone to achieve potent insulin sensitizing effects. These results suggest that such a combined approach may provide a regimen for the expanded use of TZDs in the clinic while avoiding their unwanted side effects.

RESULTS

GPR120 is a PPARγ target gene

Our previous studies showed that chow-fed GPR120 KO animals are more inflamed and insulin resistant than wild-type (WT) mice whereas ω3-FA supplementation (fish oil diet; FOD) leads to potent anti-inflammatory, insulin sensitizing effects in obese WT animals, much like the efficacy of rosiglitazone (Rosi) (Oh et al., 2010).

Here, we found that GPR120 gene (Figs. 1A and S1A) and protein expression (Fig. 1B) was increased during adipocyte differentiation and this was further enhanced by Rosi treatment. In contrast, Rosi treatment did not affect GPR120 expression in primary macrophages (Fig. 1C). Rosi treatment of HFD-fed obese mice substantially increased GPR120 expression in the adipocyte but not stromal vascular cell (SVC) fractions of epididymal white adipose tissue (eWAT) (Fig. 1D). Notably, while GPR120 expression is up-regulated in eWAT after Rosi treatment, the GPR120 expression level did not change in subcutaneous white adipose tissue (sWAT) (Fig. S1B). A similar pattern was observed for another PPARγ target gene, adiponectin, in eWAT and sWAT (Fig. S1B). Based on these data, all subsequent adipose tissue studies utilized eWAT. In patients treated with TZDs, adipose tissue expression of GPR120 was significantly increased (GSE13070; (Sears et al., 2009)) (Fig. 1E).

These results suggested that PPARγ activation leads to induction of GPR120 in adipocytes and prompted us to examine whether PPARγ is recruited to the GPR120 gene promoter. Recent reports presented genome-wide analysis of PPARγ binding during 3T3-L1 differentiation as well as in various adipose tissue depots, using Chromatin Immunoprecipitation sequencing (ChIP-seq) (Schmidt et al., 2011; Siersbaek et al., 2012; Soccio et al., 2017). Therefore, we mined published PPARγ ChIP-seq analyses of mouse adipose tissue, 3T3-L1 adipocytes, and human adipocytes from individuals with Simpson-

Golabi-Behmel Syndrome (SGBS) (GSM340799, GSM1018066, GSE92606, GSM678398). This revealed several PPARγ binding peaks in the promoter region of GPR120 in adipocytes (−878/−369, −10062/−9823, and −13903/−13664 for mouse; −212/−55, −1026/−884, −1712/−1530, and −7123/ −6571 for human), but PPARγ does not bind to those sites in macrophages (GSM532739; (Lefterova et al., 2010)) (Figs. S1H and 1F). Consistent with this, our own ChIP-PCR analysis localized PPARγ binding to two putative PPARγ response elements (PPREs) (peak 1 and peak 2 in Fig. 1F) in the promoter region of the GPR120 gene in mature 3T3-L1 adipocytes (day 8 post-differentiation, D8) (Fig. 1G). Binding to these regions in preadipocytes (D0), in which PPARγ expression is low, was negligible, serving as a negative control (Fig. 1G). These results indicate that GPR120 is a direct PPARγ target gene in adipocytes but not in macrophages.

GPR120 activation enhances PPARγ-mediated insulin sensitization

To assess whether GPR120 activation can promote PPARγ activity, we compared the expression of known PPARγ target genes (including PPARγ itself) in adipose tissue of WT mice fed with an HFD vs. HFD supplemented with ω3-FAs (FOD) or the GPR120 agonist CpdA. We found that both FOD and CpdA upregulated PPARγ, GLUT4, PEPCK, adiponectin, and adipsin gene expression in adipose tissue compared to HFD alone (Fig. S1C). Similar results were observed in 3T3-L1 adipocytes treated with the ω3-FA docosahexaenoic acid (DHA) or CpdA (Fig. S1D). In contrast, neither GPR120 agonist (*i.e.* DHA or CpdA) affected PPARγ expression in primary macrophages (Fig. S1F).

To validate these results *in vivo*, we conducted hyperinsulinemic-euglycemic clamp studies in HFD-fed obese WT and GPR120 KO mice. The treatment with a rosiglitazone food admixture (Rosi) and FOD led to the expected increase in systemic insulin sensitivity in HFD-fed WT mice as evidenced by the increase in glucose infusion rate (GIR), insulin stimulated glucose disposal rate (IS-GDR) and hepatic glucose production (HGP) suppression (Fig. 2A). FOD failed to improve insulin sensitivity in GPR120 KO animals. Notably, the insulin sensitizing effects of Rosi treatment were markedly blunted in the KO mice, indicating an interaction between GPR120 and the mechanisms of Rosi-mediated insulin sensitization.

To explore this possible interaction further, we next conducted *in vivo* studies in *ob/ob* mice treated with either Rosi, FOD, or a combination (combo) of the two (Figs. S2A–C). Figures S2A–S2C show that combination treatment improved glucose tolerance and lowered basal insulin levels more effectively than Rosi or FOD alone. The data in *ob/ob mice* show that the increased body weight and hemodilution caused by Rosi (40 mg/kg) was attenuated by adding FOD to Rosi (Fig. S2C). The above results provided a compelling rationale for further studies using various doses of Rosi, either alone or in combination with CpdA. Thus, we conducted dose-response studies in HFD-fed mice to find the minimal dose of Rosi that causes full insulin sensitivity in combination with CpdA. The different concentrations of Rosi (intermediate (mid), 10 mg/kg; and maximal (max), 40 mg/kg) were based on previous studies (Kuda et al., 2009; Kus et al., 2011; Li et al., 2011). The 40 mg/kg dose of Rosi has been widely used to achieve maximum effects in mouse models (Drosatos et al., 2013; Reifel-Miller et al., 2005), while 10 mg/kg of Rosi is the lowest concentration used in the

literature (Kuda et al., 2009; Kus et al., 2011). Based on the results of the glucose clamp studies (Figure S2F), both the maximal (40 mg/kg) and intermediate (10 mg/kg) dose of Rosi significantly increased insulin sensitivity with or without CpdA (Figs. S2D, S2F). However, the combination with CpdA led to additive metabolic improvement and prevented Rosi-mediated weight gain and hemodilution (Fig. S2E). As maximal effects of Rosi are so potent, we conducted further studies to identify a minimal Rosi dose (data not shown), to determine if it had additive effects in combination with GPR120 agonist.

Treatment with a minimal dose of Rosi (0.8 mg/kg) led to a subtle enhancement of glucose tolerance (Fig. 2B) and was less effective than CpdA treatment. Treatment with the combination of these two agonists (combo) led to an additive improvement in glucose tolerance (Fig. 2B) in WT but not in GPR120 KO mice. The same pattern was found in insulin tolerance tests (ITTs), showing a non-significant effect of Rosi alone and additive insulin sensitivity with combo treatment in WT mice but not in GPR120 KO mice (Fig. 2C). We also performed hyperinsulinemic-euglycemic clamp studies in these mice and found that the minimal dose of Rosi failed to improve the various measures of insulin sensitivity. In contrast, CpdA led to the predicted increase in insulin sensitivity, and combo produced a significant further enhancement. In contrast, none of these effects of CpdA, either alone or in combination with Rosi, were observed in GPR120 KO mice (Fig. 2D). We also measured cellular effects mediated by GPR120 stimulation in primary adipocytes with or without Rosi treatment. CpdA treatment activated insulin-independent AKT phosphorylation and pre-treatment with Rosi for 24 hr enhanced CpdA-mediated AKT phosphorylation in WT primary adipocyte, but not in GPR120 KO adipocytes (Fig. 2E). Our previous studies showed that GPR120 agonism has modest effects to increase adipocyte glucose transport and AKT phosphorylation in an insulin-independent manner and that this is mediated by Gq/11-coupled activation (Oh da et al., 2014; Oh et al., 2010). Figure S2G shows that Rosi treatment increased CpdA-mediated glucose uptake only in WT, but not in GPR120 KO, adipocytes. These results, together with the glucose clamp studies in Figure 2, indicate an interaction between GPR120-mediated and TZD-mediated insulin sensitizing actions. Notably, the minimal dose of Rosi did not cause body weight gain or hemodilution by itself or in the combination mode (Fig. S2H).

As GPR120 and PPARγ activation can each induce anti-inflammatory effects, we studied whether PPARγ activation could enhance GPR120-mediated anti-inflammatory signaling. The minimal dose of Rosi (0.8 mg/kg) was ineffective at reducing adipose tissue macrophage (ATM) infiltration or pro-inflammatory gene expression in HFD-fed mice. In contrast, CpdA treatment substantially decreased ATMs and promoted anti-inflammatory signaling (Fig. S3). Interestingly, Rosi did not augment the anti-inflammatory effects of CpdA, consistent with the lack of a Rosi effect on macrophage GPR120 expression (Figs. 1C and 1D).

Adipocyte GPR120 activation enhances PPARγ-mediated insulin sensitization

We have previously published that GPR120-mediated insulin sensitizing effects are predominantly derived through anti-inflammatory actions in macrophages and adipocytes (Oh da et al., 2014; Oh et al., 2010). Figure 2A demonstrates that deletion of GPR120

impaired the insulin sensitizing response to Rosi treatment. Figure 1C shows that, unlike in adipocytes, Rosi treatment does not enhance GPR120 expression in macrophages. Based on this information, we used LysM-Cre or adiponectin-Cre to mediate excision of GPR120 in macrophages or adipocytes, generating macrophage- (MKO) or adipocyte-selective (AKO) GPR120 KO mice. Use of these mice allowed us to distinguish the effects of GPR120 stimulation on these two cell types *in vivo* to further explore the interaction between GPR120 and PPARγ activation. Figure 3 shows that CpdA treatment improved glucose tolerance in WT mice and was much less effective in MKO mice. The effects of CpdA treatment were modestly reduced in AKO mice (Figs. 3B and 3C). Consistent with the glucose clamp data shown in Figure 2, the effect of Rosi (40 mg/kg) treatment to enhance glucose tolerance was reduced in the AKO mice compared to WT. Figure 3B shows the full effect of CpdA to improve glucose tolerance in floxed control (Fl/Fl) mice. The effects of CpdA in AKO mice were 70-80% as great as in the Fl/Fl mice, while CpdA treatment effects in the MKO mice were markedly blunted. Interestingly, unlike the results in the global GPR120 KOs (Supplemental Figure 2), combination treatment with CpdA did not prevent Rosi-mediated weight gain in MKO or AKO mice (data not shown).

Adipose tissue macrophage (ATM) infiltration was reduced by CpdA, Rosi, or combo treatment in Fl/Fl mice while CpdA had negligible effects on ATM accumulation in MKO mice (Fig. 3D). These results indicate that macrophage GPR120 largely mediates this aspect of the anti-inflammatory effects of CpdA, as previously demonstrated (Oh da et al., 2014; Oh et al., 2010). Moreover, these anti-inflammatory effects of CpdA and Rosi are independent from each other, as Rosi treatment reduced ATM infiltration in MKO comparable to its effects in Fl/Fl mice. In AKO mice, Rosi or combination treatment had comparable effects as in Fl/Fl mice, while the effects of CpdA alone were reduced by ~80% (the residual effect of CpdA is due to loss of effects on ATM accumulation exerted through adipocytes).

GPR120 stimulation decreases PPARγ-S273 phosphorylation

The transcriptional activity of PPARγ is modulated by various post-translational modifications, including phosphorylation at serine 112 and 273 (Ahmadian et al., 2013; Banks et al., 2015; Choi et al., 2010; Hu et al., 1996; van Beekum et al., 2009). Dephosphorylation of PPARγ-S273 upon agonist treatment confers an active transcriptional program that enhances insulin sensitivity (Banks et al., 2015; Choi et al., 2010; Choi et al., 2011). Both FOD or CpdA treatment increased PPARγ mRNA (Fig. S1C) and protein expression in adipose tissue of WT but not GPR120 KO mice (Figs. 4A and 4B). We observed a marked decrease in phospho-PPARγ-S273 in Rosi, FOD, and CpdA-treated WT adipose tissue (Fig. 4A), whereas PPARγ-S112 phosphorylation was not altered by GPR120 stimulation (Fig. S4A). This GPR120 stimulated decrease in phospho-PPARγ-S273 was also observed in MKO adipose tissue, while there was no reduction of phospho-PPARγ-S273 in AKO adipose tissue (Fig. S5A). These results indicate that GPR120 stimulation can enhance intrinsic PPARγ activity by modulating its phosphorylation status exclusively in adipocytes. As previously reported (Banks et al., 2015; Choi et al., 2010; Choi et al., 2011), PPARγ-S273 dephosphorylation in adipocytes does not affect adipogenic capacity, but does alter the expression of a subset of target genes dysregulated in obesity, including the insulin

sensitizing adipokines, adiponectin and adipsin. Accordingly, we found that CpdA led to increased serum adiponectin levels, as well as increased adiponectin and adipsin mRNA expression in eWAT, and 3T3-L1 adipocytes (Figs. S1C, S1D, and S1E). Interestingly, kinases implicated in PPARγ-S273 phosphorylation, e.g. CDK5 (Fig. S4B) and ERK (Fig. 4C), were not inhibited by GPR120 agonists in adipose tissue. Indeed, GPR120 activation increased ERK phosphorylation in eWAT from WT mice, but not from GPR120 KO mice (Fig. 4C).

GPR120-induces biphasic ERK stimulation and modulates PPARγ-S273 phosphorylation

The findings that GPR120 stimulation did not inhibit CDK5 activity (Fig. S4B) and actually increased ERK phosphorylation (Fig. 4C) were further explored. GPR120 is coupled to Gq/11, leading to increased intracellular levels of Ca^{2+} along with PKC and ERK stimulation. We speculated that GPR120 stimulation, despite activating ERK, blocks this kinase's ability to phosphorylate PPARγ at S273. Thus, we assessed the kinetics of ERK activation following DHA (100 μM) or CpdA (10 μM) treatment of 3T3-L1 adipocytes. Both GPR120 agonists led to biphasic ERK phosphorylation, including an acute (2-5 min) and a delayed (>30 min) activation phase (Fig. 5A). This pattern is consistent with earlier findings that GPCR stimulation activates ERK by acute state G protein-mediated (*i.e.*, by Gq/11) and steady-state β arrestin-mediated signaling pathways (Ahn et al., 2004; Tohgo et al., 2003; Tohgo et al., 2002; Wei et al., 2003). To further explore this biphasic response, we measured the kinetics of DHA-induced ERK phosphorylation (0, 2, 5, 10, 20, 30, and 60 min) in 3T3-L1 adipocytes with or without Gq/11 or β arrestin-2 knockdown (Figs. 5B and 5C). We found that Gq/11-mediated ERK phosphorylation is rapid and transient, while β arrestin-2-mediated ERK phosphorylation is delayed and sustained (Figs. 5B and 5C).

It is known that TNFα treatment of 3T3-L1 adipocytes leads to PPARγ-S273 phosphorylation via the CDK5-ERK axis (Banks et al., 2015; Choi et al., 2010; Choi et al., 2011). TNFα strongly stimulated phosphorylation of ERK, as well as PPARγ-S273 (Fig. 5D). In contrast, GPR120 agonists stimulated ERK phosphorylation but decreased PPARγ-S273 phosphorylation in WT adipose tissue (Fig. 4). PPARγ-S273 phosphorylation induced by TNFα (50 ng/ml for 30 min) was blocked by 100 μM DHA or 10 μM CpdA pretreatment at 60 min (reflecting β arrestin-2-dependent ERK activation) (Fig. 5E), but not at 2 min (reflecting Gq/11-dependent ERK activation) (Fig. 5F).

GPR120 stimulation modulates PPARγ phosphorylation via β arrestin-2 association with ERK

In the unstimulated state, β arrestin-2 largely associates with the actin cytoskeleton in the cytosol (Shenoy and Lefkowitz, 2011). After GPR120 activation, β arrestin-2 associates with GPR120, the complex then internalizes, which brings β arrestin-2 into physical proximity with ERK (Ahn et al., 2004; Ge et al., 2003; Luttrell et al., 2001). At this point, β arrestin-2 directly binds to ERK in a GPR120-dependent manner (Fig. 6A) sequestering ERK in the cytosol and preventing its nuclear translocation (Figs. 6B and 6C). We have measured β arrestin-2 and ERK localization by immunocytochemistry in HEK293 cells transfected with GPR120 (Figs. 6D and S6). When GPR120 is stimulated, cytosolic β arrestin-2 migrates towards the plasma membrane and interacts with GPR120 and becomes internalized (Fig.

S6A; (Oh et al., 2010)). Consistent with the co-immunoprecipitation assays in Figures 6A–6C, we found that GPR120 stimulation activates ERK, causing its colocalization with β arrestin-2 and retention in the cytoplasm (Figs. 6D and S6B). In contrast, the potent ERK activators phorbol 12-myristate 13-acetate (PMA) and TNFα induce activation and nuclear translocation of ERK. After GPR120 activation (by DHA or CpdA), the direct association between β arrestin-2 and ERK blocked TNFα-induced ERK nuclear translocation and inhibited subsequent PPARγ S273 phosphorylation in primary adipocytes isolated from WT mice but not β arrestin-2 KO mice (Fig. 6E). The schematic model for this mechanism is described in Figure S6C.

GPR120 stimulation induces the endogenous PPARγ ligand 15d-PGJ2

We have previously reported that GPR120 activation inhibited the conversion of arachidonic acid (AA) into pro-inflammatory eicosanoids such as LTA4, LTB4, PGE2, and PGF2 (Oh da et al., 2014; Oh et al., 2010). As the anti-inflammatory eicosanoid 15-deoxy$\Delta^{12,14}$-prostaglandin J2 (15d-PGJ2) has been identified as an endogenous PPARγ ligand (Forman et al., 1995; Kliewer et al., 1995; Ray et al., 2006; Wayman et al., 2002), we measured its adipose tissue levels in FOD- and CpdA-treated WT and GPR120 KO mice. Adipose tissue 15d-PGJ2 levels were increased following GPR120 agonist treatment in WT but not in GPR120 KO mice (Fig. 7A). We also measured 15d-PGJ2 levels in media conditioned by primary adipocytes treated with or without DHA or CpdA. Consistent with the results in Figure 7A, GPR120 stimulation increased 15d-PGJ2 levels in conditioned media (CM) from WT but not GPR120 KO adipocytes (Fig. 7B). The levels of 15d-PGJ2 as well as its precursor PGD2 were also increased in the CM from 3T3-L1 adipocytes treated with DHA or CpdA (Figs. 7C and S7B). These CM were used to treat HEK293 cells after transient co-transfection with a PPRE-driven luciferase reporter (3X-PPRE-TK-LUC; PPRE-luc), PPARγ, and RXR. CM from GPR120 agonist treated cells led to an increase in PPRE-luc activity (Fig. 7D). Inhibition of 15d-PGJ2 synthesis by the prostaglandin D synthase (PGDS) inhibitor blocked the effects of GPR120 stimulation to increase 15d-PGJ2 levels (Fig. S7C) and CpdA-mediated upregulation of PPARγ target genes in 3T3-L1adipocytes (Fig. S7D) as well as CM stimulated PPRE-luc activity (Fig. S7E). We also observed that 15d-PGJ2 (30 μM) treatment decreased TNFα-induced PPARγ-S273 phosphorylation in 3T3-L1 adipocytes, comparable to the effects of Rosi (Fig. 7E).

PPARγ ligand treatment causes dissociation of PPARγ from NCoR, a major co-repressor (Li et al., 2011; Yu et al., 2005). We have previously shown that NCoR binds to PPARγ and promotes CDK5-mediated S273 phosphorylation (Li et al., 2011). Figure 7F shows that 15d-PGJ2 treatment of 3T3-L1 adipocytes dissociated NCoR from the PPARγ transcriptional complex, comparable to the effects of Rosi. Similar results were seen *in vivo,* where Rosi or GPR120 stimulation led to decreased PPARγ association with NCoR (Fig. 7G) and CDK5 (Fig. 7H). Similar findings were obtained using a two-hybrid assay in HEK293 cells (Figs. S7F and S7G). Together, these data provide an additional mechanism for the GPR120-dependent decrease in PPARγ-273 phosphorylation.

DISCUSSION

Based on the known effects of PPARγ agonists (*i.e.*, rosiglitazone) and GPR120 agonists (*i.e.*, ω3-FAs and CpdA) to improve glucose tolerance and insulin sensitivity in obese mice, we assessed the interaction between these two pathways. The main findings are that the combination of Rosi and GPR120 agonists was more potent than either compound alone in improving glucose tolerance and insulin sensitivity. This interaction is particularly notable in obese mice treated with a low dose (0.8 mg/kg) of Rosi that, by itself, had negligible effects on glucose homeostasis. We also identified the underlying mechanisms of this positive reinforcing system. We found that GPR120 is a direct PPARγ target gene in adipocytes, explaining why TZD treatment enhances the effects of GPR120 agonists. In addition, GPR120 stimulation increases TZD activity by decreasing PPARγ S273 phosphorylation and increasing cellular content of the PPARγ ligand 15d-PGJ2. Beyond these molecular mechanisms, *in vivo* studies in AKO and MKO mice show that the majority of the effects of CpdA are mediated through anti-inflammatory actions in macrophages. In contrast, Rosi works largely in adipocytes and CpdA + Rosi treatment causes additive insulin signaling in adipocytes. Harnessing the effects of these two cell types together *in vivo* allows combination treatment to produce more robust effects to mitigate insulin resistance and improve glucose metabolism. Taken together, these studies suggest the therapeutic potential of combining GPR120 and PPARγ agonism to achieve greater metabolic benefit on glucose tolerance and insulin sensitivity. In addition, the ability to use low doses of TZDs will likely mitigate their adverse effects and increase safety.

PPARγ is a well-studied key regulator of adipocyte differentiation and function, and the TZD class of agonists has well known anti-diabetic, insulin sensitizing effects in man (Imai et al., 2004; Lehmann et al., 1995; Tontonoz et al., 1994; Tontonoz and Spiegelman, 2008; Yki-Jarvinen, 2004), but their clinical use (notably, Pioglitazone and Rosiglitazone) is limited by adverse effects. GPR120 is a key membrane receptor for ω3-FAs and is abundantly expressed in adipocytes, macrophages, other immune cells and elsewhere (Ichimura et al., 2012; Oh da et al., 2014; Oh et al., 2010; Paulsen et al., 2014). We have shown that ω3-FAs and a small molecule GPR120 agonist (CpdA) produces potent anti-inflammatory and insulin sensitizing effects on macrophages and adipocytes both *in vitro* and *in vivo* (Oh da et al., 2014; Oh et al., 2010). Thus, GPR120 agonism in obesity leads to decreased accumulation of ATMs with a marked reduction in their inflammatory program with a subsequent increase in insulin sensitivity. GPR120 agonists also work directly on adipocytes to increase glucose uptake and improve insulin sensitivity.

Previous studies have suggested that treatment with either ω3-FAs or high-dose Rosi can ameliorate adipocyte hypertrophy and insulin resistance in mice (Kuda et al., 2009; Kus et al., 2011). In addition, the combination of ω3-FAs with Rosi led to a greater increase in adiponectin secretion from human adipocytes than either agent alone (Tishinsky et al., 2011). These studies, combined with the concept that PPARγ and GPR120 agonists use discrete pathways to improve insulin sensitivity, prompted us to explore the effects and mechanisms of combination treatment. The current studies indicate that combination treatment has positive interacting effects suggesting the possibility of therapeutic benefit.

Based on our glucose clamp data, it is clear that GPR120 agonists have robust effects to improve insulin sensitivity (GIR, IS-GDR, or HGP suppression) in WT mice, but are without effect in GPR120 KO mice. With respect to the additivity concept, it is also clear that the effects of Rosi on all of these clamp-based aspects of insulin sensitivity are dramatically reduced in the GPR120 KO mice. These data point to a positive interaction between these 2 signaling systems. Consistent with this, FOD + Rosi treatment had a greater effect to improve glucose tolerance in *ob/ob* mice than FOD or Rosi alone. To explore this further, we treated HFD-fed obese mice with the small molecule GPR120 agonist CpdA and with Rosi. In these studies, our first goal was to titrate down the dose of Rosi to identify a low dose with negligible metabolic effects in order to better demonstrate additivity in combination with CpdA. From a clinical translational point of view this is a key issue, as lowering the dose of a TZD while maintaining maximal insulin sensitizing efficacy is an important means to mitigate unwanted side effects. Indeed, our glucose clamp data demonstrate that combination treatment with CpdA + minimal-dose Rosi gives the same full degree of insulin sensitization as the maximal dose of Rosi. Moreover, as measured by GTTs and ITTs we found additive effects of combination treatment over either monotherapy. As we found by hyperinsulinemic-euglycemic clamp, we again observed additivity in the combination treatment group compared to Rosi or CpdA alone. In this case, the effects of the minimal dose of Rosi are small to negligible with respect to GIR, IS-GDR, HGP suppression, and FFA suppression. When Rosi is used in combination with the GPR120 agonist there is a clear and statistically significant enhancement of insulin sensitivity across all the measurements, comparable to the maximal dose of Rosi. Thus, combination therapy produced highly effective metabolic benefits.

Our studies on the new models in which GPR120 is specifically deleted in macrophages (MKOs) or adipocytes (AKOs) have allowed us to expand this concept in an additional direction. For example, we have performed multiple GTTs in these new mouse models in combination mode or with either drug alone. In the AKO mice the beneficial effects of CpdA are only modestly less when compared to Fl/Fl mice, indicating that a major effect of the GPR120 agonist to improve insulin sensitivity is mediated through anti-inflammatory effects in the macrophages. This was confirmed in the MKO mouse studies, which show a more marked reduction in CpdA effects. With respect to interaction between these 2 signaling systems, the effects of Rosi or combination therapy are significantly less in AKO mice compared to Fl/Fl mice and we interpret this to mean that without adipocyte GPR120, Rosi is less effective and the adipocyte actions of CpdA are absent. From the combination studies in these mice, we infer that 20-30% of the overall insulin sensitizing effects of GPR120 agonists are attributable to positive interacting effects with rosiglitazone in adipocytes.

The results with MKO mice are also quite interesting and consistent with these concepts. In our previous studies, we showed that the CpdA effect on macrophages to cause insulin sensitivity is due to its anti-inflammatory actions. Here we find that the effects of CpdA to improve glucose tolerance are 70-80% reduced when macrophage GPR120 is deleted. On the other hand, the effects of rosiglitazone are preserved (please note that these studies were performed with maximum doses of rosiglitazone in order to see the full TZD effect). From these studies we suggest that 70-80% of the effect of CpdA alone to improve insulin

sensitivity is mediated through macrophage GPR120, with the remaining effect mediated through adipocyte GPR120. Therefore, in the *in vivo* setting, much of the additivity between these two agonists is because they are working on different cell types. GPR120 works mainly by inhibiting inflammatory pathways in macrophages, whereas, TZDs work mainly in adipocytes. Harnessing the effects on the two cell types together provides additional beneficial metabolic effects and the MKO and AKO models have allowed us to highlight this *in vivo* physiologic mechanism. In addition, there is an element of cell autonomous additivity in adipocytes between the two molecular signaling systems. For example, we show that the effects of CpdA to increase AKT phosphorylation and to stimulate primary adipocyte glucose transport are greater when used in combination with rosiglitazone.

It is known that PPARγ activity is inhibited by S273 phosphorylation (Banks et al., 2015; Choi et al., 2010; Choi et al., 2011). Our studies show that both Rosi and CpdA led to decreased PPARγ-S273 phosphorylation, which may contribute to the positive cross-talk between these two receptor signaling systems in adipocytes. In whole adipose tissue, PPARγ-S273 phosphorylation almost entirely reflects adipocytes, as we found here that adipocyte expression of PPARγ is ~60 fold greater than expression levels in macrophages (Fig. S1G).

We further show that this effect of CpdA on PPARγ-S273 phosphorylation was mediated by two separate mechanisms. Firstly, GPR120 agonism can couple into a β arrestin-2 signaling pathway, and secondly GPR120 stimulation led to enhanced steady-state activation of ERK, a kinase responsible for PPARγ-S273 phosphorylation. We speculated that while GPR120 signaling enhances ERK activity, it actually prevents it from phosphorylating PPARγ. Thus, CpdA causes association of GPR120 with β arrestin-2, followed by direct β arrestin-2 binding to ERK, and sequestering this kinase in the cytosol. Thus, GPR120 stimulation inhibits the nuclear translocation of activated ERK, preventing PPARγ-S273 phosphorylation. This block maintains PPARγ in a relatively unphosphorylated state and enhances its transcriptional program.

In addition to this effect on the ERK pathway, other mechanism might be at play that regulate PPARγ-S273 phosphorylation by GPR120 signaling. For example, a recent study (Khim et al., 2020) demonstrated that the protein phosphatase PPM1A interacts with PPARγ and directly dephosphorylates S273. Moreover, PPM1A expression negatively correlates with the degree of PPARγ phosphorylation, both in HFD-fed obese mice and human adipose tissue. It is possible that this mechanism, at least in part, mediates CpdA-induced PPARγ-S273 dephosphorylation.

As an additional mechanism, GPR120 stimulation led to the induction of an endogenous PPARγ ligand, 15d-PGJ2, in adipose tissue *in vivo* and in adipocytes *in vitro* in WT, but not in GPR120 KO cells. Although 15d-PGJ2 can clearly stimulate PPARγ, its physiological and pharmacological relevance has been debated (Bell-Parikh et al., 2003; Powell, 2003). For example, the concentrations required to activate PPARγ are generally reported in the μM range, while endogenous prostaglandins often act at low nM concentrations. Consistent with this, we were unable to detect 15d-PGJ2 in mouse plasma (data not shown). However, 15d-PGJ2 acts intracellularly to activate PPARγ, in contrast to other prostaglandins that

principally act as extracellular ligands of cell surface receptors. Here, we show that GPR120 stimulation strongly induces 15d-PGJ2 in macrophages as well. This raises the possibility that local secretion of 15d-PGJ2 from macrophages *in vivo* could activate PPARγ in nearby adipocytes *(i.e.,* by paracrine effects). Thus, the microenvironment concentration of 15d-PGJ2 is higher than circulating levels which seem to be sufficient to activate PPARγ and/or block phosphorylation of PPARγ. Consistent with this concept, we find that the levels of 15d-PGJ2 are increased in CM from CpdA- and DHA-treated cells and that CpdA and DHA do not increase 15-PGJ2 levels in GPR120 KO cells. Importantly, we also show that the CpdA- and DHA-stimulated CM is sufficient to directly activate PPARγ in a PPRE-transcriptional assay. Furthermore, inhibition of PGDS blocked all of these effects. Collectively, these results indicate that 15d-PGJ2 can activate PPARγ under the conditions of our study, but future studies on this subject are warranted. Lastly, we found that GPR120 induced 15d-PGJ2 and like Rosi this leads to PPARγ-S273 dephosphorylation and dissociation of PPARγ from the co-repressor NCoR, consistent with the interaction of GPR120 and Rosi signaling. In AKO adipose tissue, the effect of Rosi to cause dissociation of NCoR from PPARγ is blunted and the effect of CpdA is absent. As the GPR120 agonist promotes generation of endogenous PPARγ ligands within adipocytes, it is reasonable to suspect that deletion of GPR120 would weaken the endogenous agonist input to PPARγ:NCoR dissociation. As dephosphorylated PPARγ-S273 is transcriptionally more activate and promotes insulin sensitivity, these findings provide additional insight into why the effects of rosiglitazone are reduced in the absence of GPR120 agonism in adipocytes and why they are restored when adipocyte GPR120 is present.

Our studies in mice show that combo treatment with GPR120 and PPARγ agonists allowed use of a much lower dose of Rosi. It is possible that such a combination may be leveraged to minimize TZD-induced side effects such as edema (Basu et al., 2006; Berria et al., 2007; Nesto et al., 2004), weight gain (Choi et al., 2010; Fonseca, 2003; Lu et al., 2011; Nesto et al., 2004), bone loss (Bray et al., 2013; Colhoun et al., 2012), and possibly heart disease (Duan et al., 2005; Lago et al., 2007; Son et al., 2007). Indeed, we found that co-treatment with GPR120 agonists prevented high-dose Rosi from causing weight gain and fluid retention in mice, and the low dose of Rosi used did not induce these side effects. This finding raises the possibility that other potential TZD-mediated side effects, not measured in our studies, might also be reduced at low-dose TZD treatment. TZD-mediated weight gain is due to increased food intake and adipogenesis; thus, we have measured whether GPR120 activation has any effect on food intake and did not find any notable differences. Understanding how GPR120 stimulation reduces Rosi-mediated weight gain and hemodilution would be an important translational point. Interestingly, recent reports raised the possibility that high expression and sensitivity of the GPR120 pathway in brown fat (Quesada-Lopez et al., 2016; Schilperoort et al., 2018) might be one of the mechanisms to prevent PPARγ-mediated weight gain. In addition, it has also been shown that GPR120 activation in osteoblasts inhibits osteoclastogenesis (Ahn et al., 2016; Cornish et al., 2008). Thus, it would be of interest to learn whether the combination of GPR120 agonist and minimal dose Rosi treatment can avoid high-dose Rosi-mediated bone loss.

In summary, the current studies show a positive interaction between GPR120 and PPARγ agonism to promote glucose tolerance and insulin sensitivity in obese mice. Mechanistically,

we established that GPR120 is a direct PPARγ target gene, providing a rationale for TZD-enhanced GPR120 signaling. In addition, GPR120 activation stimulates the production of the PPARγ ligand, 15d-PGJ2 in adipocytes and also blocks the inhibiting ERK-mediated phosphorylation of PPARγ-S273. *In vivo*, a major component of the additivity is the combination of CpdA anti-inflammatory actions in macrophages coupled with the effects of both ligands in adipocytes. Lastly, if concomitant GPR120 agonism could reduce unwanted TZD side effects either by direct actions or by allowing lower doses of TZDs, then this could have substantial clinical importance.

LIMITATIONS OF STUDY

Although we used the maximum doses of rosiglitazone to see the full TZD effects in combination studies using GPR120 MKO and AKO mice, it would be of interest to assess combination studies with the minimal dose of rosiglitazone in these tissue-specific GPR120 KO mice in the future. In addition, future studies on the role of 15d-PGJ2 as an endogenous PPARγ activator will be of interest, particularly related to bioactive intracellular and microenvironmental concentrations. Finally, these studies do not identify the mechanisms whereby CpdA blocks the adverse effects of Rosi-induced weight gain and hemodilution, and such studies will be important with respect to the potential translation of our findings to humans.

STAR METHODS

RESOURCE AVAILABILITY

Lead Contact—Further information and requests for resources and reagents should be directed to and will be fulfilled by the Lead Contact, Da Young Oh, PhD (UT Southwestern Medical Center, dayoung.oh@utsouthwestern.edu).

Materials Availability—Mouse lines generated in this study (GPR120 tissue specific KO mice and GPR120 Fl/Fl mice) are restricted to share with 3rd party under licensing agreement with Merck & Co..

Data and Code Availability—The published article includes all datasets generated or analyzed during this study.

EXPERIMENTAL MODEL AND SUBJECT DETAILS

Animal care and use—The generation of GPR120 KO mice has been previously described (Oh da et al., 2014; Oh et al., 2010). GPR120 Fl/Fl mice were provided by Taconic, Inc. under the licensing agreement with Merck & Co.. GPR120 Fl/Fl mice were bred with adiponectin-Cre mice (obtained from Dr. Philipp Scherer's lab at UTSW) to generate adipocyte-specific GPR120 KO (AKO) or Lys M-Cre mice (kindly provided by Dr. Chris Glass' lab at UCSD) to generate macrophage-specific GPR120 KO (MKO) mice. All mice were maintained on a 12/12 hr light-dark cycle. Animals were housed in a specific pathogen-free facility and given free access to food and water. All procedures were approved by the University of California San Diego and UT Southwestern Medical Center animal care and use committee. Male *ob/ob* mice were fed a HFD (60% fat calories, 20% protein

calories, and 20% carbohydrate calories; Research Diets) *ad libitum* for 10 days from 6 weeks of age and then switched to a Rosi-supplemented HFD (40 mg/kg of diet) with or without an isocaloric HFD supplemented with ω3-FAs concentrate (FOD) for 2 weeks. Male C57BL/6J WT and GPR120 KO littermates were fed an HFD *ad libitum* for 15-20 weeks from 8 weeks of age. After 15 weeks of HFD feeding, WT and GPR120 KO mice were switched to either FOD or 0.8 mg/kg Rosi (minRosi), 10 mg/kg Rosi (midRosi) or 40 mg/kg Rosi (maxRosi) with or without 45 mg/kg of CpdA (CpdA) administered HFD for 5 weeks. GPR120 Fl/Fl, MKO and AKO mice were fed an HFD *ad libitum* for 15-20 weeks from 8 weeks of age. After 15 weeks of HFD feeding, mice were switched to 40 mg/kg Rosi (maxRosi) with or without 45 mg/kg of CpdA (CpdA) administered HFD for 5 weeks. All diets were custom made from Research Diets. Mice received fresh diet every 3rd day, and food consumption and body weight were monitored. Male WT and β arrestin-2 KO mice were fed a normal chow diet (13.5% fat; LabDiet). *In vivo* metabolic studies were performed as described previously (Oh da et al., 2014; Oh et al., 2010).

Cell lines—To generate adipocytes, 3T3-L1 cells (ATCC, not authenticated) were cultured in medium (Dulbecco's modified Eagle's medium (DMEM) containing 10% FBS, penicillin-streptomycin, and glutamine) until confluent, and then induced with a differentiation cocktail consisting of 0.5 mM of 3-isobutyl-1-methylxanthine, 1 mM dexamethasone, 10 mg/mL insulin, 0.2 mM indomethacin in DMEM supplemented with 10% FBS, penicillin-streptomycin, and glutamine) for 7-10 days.

METHODS DETAILS

Glucose tolerance and insulin tolerance tests and hyperinsulinemic-euglycemic clamp studies—For GTTs, mice received one dose of dextrose (1.5 g/kg body weight) via *i.p.* injection after 6 hr of fasting. For ITTs, mice were fasted for 6 hr and then *i.p.* injected with insulin (0.70 units/kg body weight). To perform hyperinsulinemic-euglycemic clamp assays, dual catheters (MRE-025, Braintree Scientific) were implanted in the right jugular vein and tunneled subcutaneously and exteriorized at the back of the neck. Three to five days after recovery, 6 hr fasted mice were infused with D-[3-^{3}H] glucose (Perkin Elmer) for 90 min. After tracer equilibration, blood sampling occurred, then glucose (50% dextrose) and tracer (5 μCi/h) plus insulin (8 mU/kg/min) were infused into the jugular vein. Blood samples were measured from the tail vein at 10 min intervals. The steady-state conditions (120 mg/dl ± 10 mg/dl) was confirmed at the end of the clamp by maintaining glucose infusion and plasma glucose concentration for a minimum of 20 min. Blood samples at time point = 10, 0 (basal), 110, and 120 (end of experiment) min were collected to determine glucose-specific activity, as well as free fatty acid and insulin concentration. At the end of the clamp period, the mice were exsanguinated by cardiac puncture (≥1 ml, whole blood collected), and tissues were harvested, mass recorded, and preserved as required for future analysis. Tracer-determined rates were quantified by using the Steele equation for steady-state conditions. At steady state, the rate of glucose disappearance (GDR) is equal to the sum of the rate of endogenous glucose productions (HGP) plus the exogenous GIR. Insulin-stimulated (IS)-GDR is equal to the total GDR minus the basal glucose turnover rate.

Chromatin Immunoprecipitation (ChIP) assay—Fully differentiated 3T3-L1 adipocytes (D8) and preadipocyte (D0) lysates were prepared using manufacturer's protocol (EpiTect ChIP One Day Kit, Qiagen). Briefly, cross-linked chromatin was sonicated and 5 μg of antibody was used: normal rabbit IgG and PPARγ antibodies. The promoter regions of GPR120 for PPARγ binding were amplified using PCR with reverse transcription (RT-PCR). For the primers used for GPR120 promoters, see Table S1.

Isolation and culture of primary adipocytes—Eight to 9-week-old WT male C57BL6/J mice, β arrestin-2 KO mice, or WT and GPR120 KO mice fed different diet treatments were used to obtain primary adipocytes as described previously (Malide et al., 2000). Briefly, the epididymal fat pads were removed, minced in the isolation buffer (PBS + 1% low endotoxin BSA) and digested using collagenase II (1 mg/ml, Sigma-Aldrich) at 37°C for 30 min, and then were filtered through cell strainer (100 μm pore size; BD Bioscience). After centrifugation at 500 g for 5 min, the supernatant containing adipocytes and pellet the stromal vascular cells (for differentiation study) were collected and then washed extensively and incubated at 37°C in DMEM containing 5% BSA. Primary adipocytes and CM were taken at various times with treatments as indicated in the figure legends and were flash-frozen in liquid nitrogen and stored in −80°C until use. For *in vitro* differentiation of adipose stromal vascular fraction, the collected stromal vascular cell pellets were re-suspended in growth media containing DMEM/F12 (Invitrogen) plus 10% fetal bovine serum (FBS) and plated onto collagen-coated dishes and cultured in 10% CO_2 at 37 °C until confluency. Confluent cultures were stimulated with adipogenic cocktail (growth media supplemented with 5μg/ml insulin, 1 μM dexamethasone, and 0.5 mM isobutylmethyxanthine) for 48 h. Subsequently, cells were maintained in growth media supplemented with 5 μg/ml insulin and treated with or without 1 μM Rosi at indicated time course during differentiation.

RNA isolation and Real-time Quantitative RT-PCR—Total RNA was extracted from adipose tissue, primary adipocytes and 3T3-L1 adipocytes using an RNA purification kit (Qiagen). First-strand cDNA was synthesized using SuperScript III and random hexamers. Quantitative PCR was carried out in 20 μl reactions using iTaq SYBR Green on StepOne Real-Time PCR System (Applied Biosystems). Relative gene expression was calculated as mRNA level normalized to that of the standard housekeeping gene (GAPDH) using the ΔΔCT method. The specificity of the PCR amplification was verified by melting curve analysis of the final products using StepOne software. Primer sequences were provided in Table S1.

Protein isolation, western blots, and co-immunoprecipitation—Primary adipocytes, 3T3-L1 adipocytes, HEK293 cells or eWAT were homogenized in RIPA buffer supplemented with protease and phosphatase inhibitors. Cell or tissue lysates were subjected to western blotting and proteins were detected by corresponding antibodies. Protein bands were analyzed using densitometry and ImageJ image analysis software, normalizing phosphorylated protein to total protein. For co-immunoprecipitation, HEK293 cells, 3T3-L1 adipocytes, or eWAT were homogenized in lysis buffer (150 mM NaCl, 50 mM HEPES (pH 7.4), 1 mM EDTA, 1% NP-40 with protease and phosphatase inhibitors), and lysates were

incubated with anti-β arrestin-2 (2 μg), anti-NCoR (5 μg), or anti-PPARγ (5 μg) antibody overnight for 4°C and immune complexes precipitated with magnetic protein A Dynabeads for 3 hr at 4°C. Beads were washed with PBS and resuspended in sample buffer. Lysates and immune complexes were separated by SDS-PAGE for western blotting.

Immunocytochemistry and confocal microscopy—HEK293 cells were used for immunocytochemistry using confocal microscopy. For visualization of Flag-GPR120 and GFP-β arrestin-2, transiently transfected HEK293 cells on Poly-L-Lysine coated coverslips in 24 well plates were stimulated as described in the figure legends, washed with PBS, fixed with 10% paraformaldehyde for 30 min at room temperature, and again washed with PBS prior to examination. Cells were incubated with a 1:500 dilution of mouse anti-Flag antibody in 1% BSA/PBS for overnight at 4°C, and washed three times with PBS, and then incubated with anti-mouse IgG secondary antibody conjugated Alexa Fluor 546 for 30 min at room temperature. Cells were washed three times with PBS prior to examination. For visualization of GFP-β arrestin-2 and RFP-ERK2, transiently transfected HEK293 cells on Poly-L-Lysine coated coverslips in 24 well plates were stimulated as described in the figure legends, washed with PBS, fixed with 10% paraformaldehyde for 30 min at room temperature, and again washed with PBS prior to examination. The samples were analyzed by confocal microscopy by using Olympus Fluoview 1000.

Eicosanoid measurements—15d-PGJ2 and PGD2 were directly quantified in the CM from 3T3-L1 adipocytes or primary adipocytes. Cells were treated as described in the figure legends, and CM were subjected to ELISA according to the manufacturer's instructions (see Key Resource Table). For adipose tissue 15d-PGJ2 measurement, mouse adipose tissue from NC, HFD, FOD, or CpdA fed WT and GPR120 KO mice were harvested and snap frozen in liquid nitrogen and stored −80°C until use. 15d-PGJ2 was measured by Liquid chromatography-mass spectrometry (LC-MS) as previously described (Quehenberger et al., 2010).

Mammalian two-hybrid assays—Following a published protocol (Fan et al., 2009; Li et al., 2011), HEK293 cells in 24 well plates were co-transfected with a DNA mixture consisting of 100 ng of pG5-Luc, 100 ng of VP16-fusion, 100 ng of Gal4-fusion, and 100 ng of GPR120 or 100 ng of NCoR and treated for 24 hr with Rosi (1 μM), DHA (100 μM) or CpdA (10 μM) as indicated prior to the luciferase assay. A human PPARγ2 cDNA was fused to VP16 or Gal4 to make VP-16 PPARγ or Gal4-PPARγ, respectively. A human CDK5 cDNA was fused to Gal4 to generate Gal4-CDK5. Full length human NCoR cDNA was fused to VP16 to make VP16-NCoR. Combinations of the constructs as described in Figure S7 and the luciferase reporter assay was used to quantitate interactions between the different proteins.

QUANTIFICATION AND STATISTICAL ANALYSIS

Data are presented as the mean ± SEM. The significance of differences between groups was evaluated using analysis of variance. The P value < 0.05 was considered significant. Statistical parameters including the exact value of n, the definition of center, dispersion and precision measures (mean ± SEM) and statistical significance are reported in the Figures and

the Figure Legends. Group sizes of 5 mice or above were sufficient to reach a statistical power of at least 80%. Mice were assigned at random to treatment groups for all mouse studies, and where possible mixed among cages. Mice that developed adverse reactions during experiments were excluded from datasets. Data is judged to be statistically significant when $P < 0.05$ by two-tailed Student's *t*-test or two-way ANOVA followed by Bonferroni's post hoc test, where appropriate. In Figures, asterisks denote statistical significance (*, $P < 0.05$). Statistical analysis was performed in GraphPad PRISM 8.

ADDITIONAL RESOURCES

The software is available on the web sites linked in the Key Resource Table.

Supplementary Material

Refer to Web version on PubMed Central for supplementary material.

ACKOWLEDGMENTS

We thank Bruce Spiegelman (Harvard Medical School) for sharing the PPARγ phosphor-S273 antibody and Robert Lefkowitz (Duke University, HHMI) for providing GFP-tagged β arrestin-2 and RFP-tagged ERK2 plasmids. We thank Angela Tyler and Jachelle Pimentel for editorial assistance, the UCSD Histology Core lab for processing adipose tissue specimens, and the UCSD Microscope Resource (funded by UCSD Neuroscience Microscopy Shared Facility Grant P30 NS047101) for confocal microscopy analysis. This work was supported by grants from the NIH (R01 DK108773 to D.Y.O.; P01DK054441, P30DK063491 to J.M.O.), the American Heart Association (14SDG19880020 to D.Y.O.), and the American Diabetes Association Minority Postdoctoral Fellowship (1-18-PMF-030 to V.A.P.).

REFERENCES

Ahmadian M, Suh JM, Hah N, Liddle C, Atkins AR, Downes M, and Evans RM (2013). PPARgamma signaling and metabolism: the good, the bad and the future. Nat Med 19, 557–566. [PubMed: 23652116]

Ahn S, Shenoy SK, Wei H, and Lefkowitz RJ (2004). Differential kinetic and spatial patterns of beta-arrestin and G protein-mediated ERK activation by the angiotensin II receptor. J Biol Chem 279, 35518–35525. [PubMed: 15205453]

Ahn SH, Park SY, Baek JE, Lee SY, Baek WY, Lee SY, Lee YS, Yoo HJ, Kim H, Lee SH, et al. (2016). Free Fatty Acid Receptor 4 (GPR120) Stimulates Bone Formation and Suppresses Bone Resorption in the Presence of Elevated n-3 Fatty Acid Levels. Endocrinology 157, 2621–2635. [PubMed: 27145004]

Banks AS, McAllister FE, Camporez JP, Zushin PJ, Jurczak MJ, Laznik-Bogoslavski D, Shulman GI, Gygi SP, and Spiegelman BM (2015). An ERK/Cdk5 axis controls the diabetogenic actions of PPARgamma. Nature 517, 391–395. [PubMed: 25409143]

Basu A, Jensen MD, McCann F, Mukhopadhyay D, Joyner MJ, and Rizza RA (2006). Effects of pioglitazone versus glipizide on body fat distribution, body water content, and hemodynamics in type 2 diabetes. Diabetes Care 29, 510–514. [PubMed: 16505497]

Bell-Parikh LC, Ide T, Lawson JA, McNamara P, Reilly M, and FitzGerald GA (2003). Biosynthesis of 15-deoxy-delta12,14-PGJ2 and the ligation of PPARgamma. J Clin Invest 112, 945–955. [PubMed: 12975479]

Berria R, Glass L, Mahankali A, Miyazaki Y, Monroy A, De Filippis E, Cusi K, Cersosimo E, Defronzo RA, and Gastaldelli A (2007). Reduction in hematocrit and hemoglobin following pioglitazone treatment is not hemodilutional in Type II diabetes mellitus. Clin Pharmacol Ther 82, 275–281. [PubMed: 17361126]

Bray GA, Smith SR, Banerji MA, Tripathy D, Clement SC, Buchanan TA, Henry RR, Kitabchi AE, Mudaliar S, Musi N, et al. (2013). Effect of pioglitazone on body composition and bone density in

subjects with prediabetes in the ACT NOW trial. Diabetes Obes Metab 15, 931–937. [PubMed: 23551856]

Chinetti G, Fruchart JC, and Staels B (2000). Peroxisome proliferator-activated receptors (PPARs): nuclear receptors at the crossroads between lipid metabolism and inflammation. Inflamm Res 49, 497–505. [PubMed: 11089900]

Choi JH, Banks AS, Estall JL, Kajimura S, Bostrom P, Laznik D, Ruas JL, Chalmers MJ, Kamenecka TM, Bluher M, et al. (2010). Anti-diabetic drugs inhibit obesity-linked phosphorylation of PPARgamma by Cdk5. Nature 466, 451–456. [PubMed: 20651683]

Choi JH, Banks AS, Kamenecka TM, Busby SA, Chalmers MJ, Kumar N, Kuruvilla DS, Shin Y, He Y, Bruning JB, et al. (2011). Antidiabetic actions of a non-agonist PPARgamma ligand blocking Cdk5-mediated phosphorylation. Nature 477, 477–481. [PubMed: 21892191]

Colhoun HM, Livingstone SJ, Looker HC, Morris AD, Wild SH, Lindsay RS, Reed C, Donnan PT, Guthrie B, Leese GP, et al. (2012). Hospitalised hip fracture risk with rosiglitazone and pioglitazone use compared with other glucose-lowering drugs. Diabetologia 55, 2929–2937. [PubMed: 22945303]

Cornish J, MacGibbon A, Lin JM, Watson M, Callon KE, Tong PC, Dunford JE, van der Does Y, Williams GA, Grey AB, et al. (2008). Modulation of osteoclastogenesis by fatty acids. Endocrinology 149, 5688–5695. [PubMed: 18617622]

Drosatos K, Khan RS, Trent CM, Jiang H, Son NH, Blaner WS, Homma S, Schulze PC, and Goldberg IJ (2013). Peroxisome proliferator-activated receptor-gamma activation prevents sepsis-related cardiac dysfunction and mortality in mice. Circ Heart Fail 6, 550–562. [PubMed: 23572494]

Duan SZ, Ivashchenko CY, Russell MW, Milstone DS, and Mortensen RM (2005). Cardiomyocyte-specific knockout and agonist of peroxisome proliferator-activated receptor-gamma both induce cardiac hypertrophy in mice. Circ Res 97, 372–379. [PubMed: 16051889]

Fan W, Imamura T, Sonoda N, Sears DD, Patsouris D, Kim JJ, and Olefsky JM (2009). FOXO1 transrepresses peroxisome proliferator-activated receptor gamma transactivation, coordinating an insulin-induced feed-forward response in adipocytes. J Biol Chem 284, 12188–12197. [PubMed: 19246449]

Fonseca V (2003). Effect of thiazolidinediones on body weight in patients with diabetes mellitus. Am J Med 115 Suppl 8A, 42S–48S. [PubMed: 14678865]

Forman BM, Tontonoz P, Chen J, Brun RP, Spiegelman BM, and Evans RM (1995). 15-Deoxy-delta 12, 14-prostaglandin J2 is a ligand for the adipocyte determination factor PPAR gamma. Cell 83, 803–812. [PubMed: 8521497]

Ge L, Ly Y, Hollenberg M, and DeFea K (2003). A beta-arrestin-dependent scaffold is associated with prolonged MAPK activation in pseudopodia during protease-activated receptor-2-induced chemotaxis. J Biol Chem 278, 34418–34426. [PubMed: 12821670]

He W, Barak Y, Hevener A, Olson P, Liao D, Le J, Nelson M, Ong E, Olefsky JM, and Evans RM (2003). Adipose-specific peroxisome proliferator-activated receptor gamma knockout causes insulin resistance in fat and liver but not in muscle. Proc Natl Acad Sci U S A 100, 15712–15717. [PubMed: 14660788]

Heilbronn LK, and Campbell LV (2008). Adipose tissue macrophages, low grade inflammation and insulin resistance in human obesity. Curr Pharm Des 14, 1225–1230. [PubMed: 18473870]

Hu E, Kim JB, Sarraf P, and Spiegelman BM (1996). Inhibition of adipogenesis through MAP kinase-mediated phosphorylation of PPARgamma. Science 274, 2100–2103. [PubMed: 8953045]

Ichimura A, Hirasawa A, Poulain-Godefroy O, Bonnefond A, Hara T, Yengo L, Kimura I, Leloire A, Liu N, Iida K, et al. (2012). Dysfunction of lipid sensor GPR120 leads to obesity in both mouse and human. Nature 483, 350–354. [PubMed: 22343897]

Imai T, Takakuwa R, Marchand S, Dentz E, Bornert JM, Messaddeq N, Wendling O, Mark M, Desvergne B, Wahli W, et al. (2004). Peroxisome proliferator-activated receptor gamma is required in mature white and brown adipocytes for their survival in the mouse. Proc Natl Acad Sci U S A 101, 4543–4547. [PubMed: 15070754]

Khim KW, Choi SS, Jang HJ, Lee YH, Lee E, Hyun JM, Eom HJ, Yoon S, Choi JW, Park TE, et al. (2020). PPM1A Controls Diabetic Gene Programming through Directly Dephosphorylating PPARgamma at Ser273. Cells 9.

Kliewer SA, Lenhard JM, Willson TM, Patel I, Morris DC, and Lehmann JM (1995). A prostaglandin J2 metabolite binds peroxisome proliferator-activated receptor gamma and promotes adipocyte differentiation. Cell 83, 813–819. [PubMed: 8521498]

Kuda O, Jelenik T, Jilkova Z, Flachs P, Rossmeisl M, Hensler M, Kazdova L, Ogston N, Baranowski M, Gorski J, et al. (2009). n-3 fatty acids and rosiglitazone improve insulin sensitivity through additive stimulatory effects on muscle glycogen synthesis in mice fed a high-fat diet. Diabetologia 52, 941–951. [PubMed: 19277604]

Kus V, Flachs P, Kuda O, Bardova K, Janovska P, Svobodova M, Jilkova ZM, Rossmeisl M, Wang-Sattler R, Yu Z, et al. (2011). Unmasking differential effects of rosiglitazone and pioglitazone in the combination treatment with n-3 fatty acids in mice fed a high-fat diet. PLoS One 6, e27126. [PubMed: 22073272]

Lago RM, Singh PP, and Nesto RW (2007). Congestive heart failure and cardiovascular death in patients with prediabetes and type 2 diabetes given thiazolidinediones: a meta-analysis of randomised clinical trials. Lancet 370, 1129–1136. [PubMed: 17905165]

Lefterova MI, Steger DJ, Zhuo D, Qatanani M, Mullican SE, Tuteja G, Manduchi E, Grant GR, and Lazar MA (2010). Cell-specific determinants of peroxisome proliferator-activated receptor gamma function in adipocytes and macrophages. Mol Cell Biol 30, 2078–2089. [PubMed: 20176806]

Lehmann JM, Moore LB, Smith-Oliver TA, Wilkison WO, Willson TM, and Kliewer SA (1995). An antidiabetic thiazolidinedione is a high affinity ligand for peroxisome proliferator-activated receptor gamma (PPAR gamma). J Biol Chem 270, 12953–12956. [PubMed: 7768881]

Li P, Fan W, Xu J, Lu M, Yamamoto H, Auwerx J, Sears DD, Talukdar S, Oh D, Chen A, et al. (2011). Adipocyte NCoR knockout decreases PPARgamma phosphorylation and enhances PPARgamma activity and insulin sensitivity. Cell 147, 815–826. [PubMed: 22078880]

Lu M, Sarruf DA, Talukdar S, Sharma S, Li P, Bandyopadhyay G, Nalbandian S, Fan W, Gayen JR, Mahata SK, et al. (2011). Brain PPAR-gamma promotes obesity and is required for the insulin-sensitizing effect of thiazolidinediones. Nat Med 17, 618–622. [PubMed: 21532596]

Luttrell LM, Roudabush FL, Choy EW, Miller WE, Field ME, Pierce KL, and Lefkowitz RJ (2001). Activation and targeting of extracellular signal-regulated kinases by beta-arrestin scaffolds. Proc Natl Acad Sci U S A 98, 2449–2454. [PubMed: 11226259]

Malide D, Ramm G, Cushman SW, and Slot JW (2000). Immunoelectron microscopic evidence that GLUT4 translocation explains the stimulation of glucose transport in isolated rat white adipose cells. J Cell Sci 113 Pt 23, 4203–4210. [PubMed: 11069765]

Martin H (2010). Role of PPAR-gamma in inflammation. Prospects for therapeutic intervention by food components. Mutat Res 690, 57–63. [PubMed: 20973164]

Medina-Gomez G, Gray SL, Yetukuri L, Shimomura K, Virtue S, Campbell M, Curtis RK, Jimenez-Linan M, Blount M, Yeo GS, et al. (2007). PPAR gamma 2 prevents lipotoxicity by controlling adipose tissue expandability and peripheral lipid metabolism. PLoS Genet 3, e64. [PubMed: 17465682]

Nesto RW, Bell D, Bonow RO, Fonseca V, Grundy SM, Horton ES, Le Winter M, Porte D, Semenkovich CF, Smith S, et al. (2004). Thiazolidinedione use, fluid retention, and congestive heart failure: a consensus statement from the American Heart Association and American Diabetes Association. Diabetes Care 27, 256–263. [PubMed: 14693998]

Oh da Y, Walenta E, Akiyama TE, Lagakos WS, Lackey D, Pessentheiner AR, Sasik R , Hah N, Chi TJ, Cox JM, et al. (2014). A Gpr120-selective agonist improves insulin resistance and chronic inflammation in obese mice. Nat Med 20, 942–947. [PubMed: 24997608]

Oh DY, Talukdar S, Bae EJ, Imamura T, Morinaga H, Fan W, Li P, Lu WJ, Watkins SM, and Olefsky JM (2010). GPR120 is an omega-3 fatty acid receptor mediating potent anti-inflammatory and insulin-sensitizing effects. Cell 142, 687–698. [PubMed: 20813258]

Paulsen SJ, Larsen LK, Hansen G, Chelur S, Larsen PJ, and Vrang N (2014). Expression of the fatty acid receptor GPR120 in the gut of diet-induced-obese rats and its role in GLP-1 secretion. PLoS One 9, e88227. [PubMed: 24520357]

Powell WS (2003). 15-Deoxy-delta12,14-PGJ2: endogenous PPARgamma ligand or minor eicosanoid degradation product? J Clin Invest 112, 828–830. [PubMed: 12975467]

Quehenberger O, Armando AM, Brown AH, Milne SB, Myers DS, Merrill AH, Bandyopadhyay S, Jones KN, Kelly S, Shaner RL, et al. (2010). Lipidomics reveals a remarkable diversity of lipids in human plasma. J Lipid Res 51, 3299–3305. [PubMed: 20671299]

Quesada-Lopez T, Cereijo R, Turatsinze JV, Planavila A, Cairo M, Gavalda-Navarro A, Peyrou M, Moure R, Iglesias R, Giralt M, et al. (2016). The lipid sensor GPR120 promotes brown fat activation and FGF21 release from adipocytes. Nat Commun 7, 13479. [PubMed: 27853148]

Raptis DA, Limani P, Jang JH, Ungethum U, Tschuor C, Graf R, Humar B, and Clavien PA (2014). GPR120 on Kupffer cells mediates hepatoprotective effects of omega3-fatty acids. J Hepatol 60, 625–632. [PubMed: 24262133]

Ray DM, Akbiyik F, and Phipps RP (2006). The peroxisome proliferator-activated receptor gamma (PPARgamma) ligands 15-deoxy-Delta12,14-prostaglandin J2 and ciglitazone induce human B lymphocyte and B cell lymphoma apoptosis by PPARgamma-independent mechanisms. J Immunol 177, 5068–5076. [PubMed: 17015690]

Reaven GM (2005). The insulin resistance syndrome: definition and dietary approaches to treatment. Annu Rev Nutr 25, 391–406. [PubMed: 16011472]

Reifel-Miller A, Otto K, Hawkins E, Barr R, Bensch WR, Bull C, Dana S, Klausing K, Martin JA, Rafaeloff-Phail R, et al. (2005). A peroxisome proliferator-activated receptor alpha/gamma dual agonist with a unique in vitro profile and potent glucose and lipid effects in rodent models of type 2 diabetes and dyslipidemia. Mol Endocrinol 19, 1593–1605. [PubMed: 15831517]

Ricote M, Huang JT, Welch JS, and Glass CK (1999). The peroxisome proliferator-activated receptor(PPARgamma) as a regulator of monocyte/macrophage function. J Leukoc Biol 66, 733–739. [PubMed: 10577502]

Schenk S, Saberi M, and Olefsky JM (2008). Insulin sensitivity: modulation by nutrients and inflammation. J Clin Invest 118, 2992–3002. [PubMed: 18769626]

Schilperoort M, van Dam AD, Hoeke G, Shabalina IG, Okolo A, Hanyaloglu AC, Dib LH, Mol IM, Caengprasath N, Chan YW, et al. (2018). The GPR120 agonist TUG-891 promotes metabolic health by stimulating mitochondrial respiration in brown fat. EMBO Mol Med 10.

Schmidt SF, Jorgensen M, Chen Y, Nielsen R, Sandelin A, and Mandrup S (2011). Cross species comparison of C/EBPalpha and PPARgamma profiles in mouse and human adipocytes reveals interdependent retention of binding sites. BMC Genomics 12, 152. [PubMed: 21410980]

Sears DD, Hsiao G, Hsiao A, Yu JG, Courtney CH, Ofrecio JM, Chapman J, and Subramaniam S (2009). Mechanisms of human insulin resistance and thiazolidinedione-mediated insulin sensitization. Proc Natl Acad Sci U S A 106, 18745–18750. [PubMed: 19841271]

Shenoy SK, and Lefkowitz RJ (2011). beta-Arrestin-mediated receptor trafficking and signal transduction. Trends Pharmacol Sci 32, 521–533. [PubMed: 21680031]

Siersbaek MS, Loft A, Aagaard MM, Nielsen R, Schmidt SF, Petrovic N, Nedergaard J, and Mandrup S (2012). Genome-wide profiling of peroxisome proliferator-activated receptor gamma in primary epididymal, inguinal, and brown adipocytes reveals depot-selective binding correlated with gene expression. Mol Cell Biol 32, 3452–3463. [PubMed: 22733994]

Soccio RE, Li Z, Chen ER, Foong YH, Benson KK, Dispirito JR, Mullican SE, Emmett MJ, Briggs ER, Peed LC, et al. (2017). Targeting PPARgamma in the epigenome rescues genetic metabolic defects in mice. J Clin Invest 127, 1451–1462. [PubMed: 28240605]

Son NH, Park TS, Yamashita H, Yokoyama M, Huggins LA, Okajima K, Homma S, Szabolcs MJ, Huang LS, and Goldberg IJ (2007). Cardiomyocyte expression of PPARgamma leads to cardiac dysfunction in mice. J Clin Invest 117, 2791–2801. [PubMed: 17823655]

Suckow AT, Polidori D, Yan W, Chon S, Ma JY, Leonard J, and Briscoe CP (2014). Alteration of the glucagon axis in GPR120 (FFAR4) knockout mice: a role for GPR120 in glucagon secretion. J Biol Chem 289, 15751–15763. [PubMed: 24742677]

Sugii S, Olson P, Sears DD, Saberi M, Atkins AR, Barish GD, Hong SH, Castro GL, Yin YQ, Nelson MC, et al. (2009). PPARgamma activation in adipocytes is sufficient for systemic insulin sensitization. Proc Natl Acad Sci U S A 106, 22504–22509. [PubMed: 20018750]

Tishinsky JM, Ma DW, and Robinson LE (2011). Eicosapentaenoic acid and rosiglitazone increase adiponectin in an additive and PPARgamma-dependent manner in human adipocytes. Obesity (Silver Spring) 19, 262–268. [PubMed: 20814411]

Tohgo A, Choy EW, Gesty-Palmer D, Pierce KL, Laporte S, Oakley RH, Caron MG, Lefkowitz RJ, and Luttrell LM (2003). The stability of the G protein-coupled receptor-beta-arrestin interaction determines the mechanism and functional consequence of ERK activation. J Biol Chem 278, 6258–6267. [PubMed: 12473660]

Tohgo A, Pierce KL, Choy EW, Lefkowitz RJ, and Luttrell LM (2002). beta-Arrestin scaffolding of the ERK cascade enhances cytosolic ERK activity but inhibits ERK-mediated transcription following angiotensin AT1a receptor stimulation. J Biol Chem 277, 9429–9436. [PubMed: 11777902]

Tontonoz P, Hu E, Graves RA, Budavari AI, and Spiegelman BM (1994). mPPAR gamma 2: tissue-specific regulator of an adipocyte enhancer. Genes Dev 8, 1224–1234. [PubMed: 7926726]

Tontonoz P, and Spiegelman BM (2008). Fat and beyond: the diverse biology of PPARgamma. Annu Rev Biochem 77, 289–312. [PubMed: 18518822]

van Beekum O, Fleskens V, and Kalkhoven E (2009). Posttranslational modifications of PPAR-gamma: fine-tuning the metabolic master regulator. Obesity (Silver Spring) 17, 213–219. [PubMed: 19169221]

Wayman NS, Hattori Y, McDonald MC, Mota-Filipe H, Cuzzocrea S, Pisano B, Chatterjee PK, and Thiemermann C (2002). Ligands of the peroxisome proliferator-activated receptors (PPAR-gamma and PPAR-alpha) reduce myocardial infarct size. FASEB J 16, 1027–1040. [PubMed: 12087064]

Wei H, Ahn S, Shenoy SK, Karnik SS, Hunyady L, Luttrell LM, and Lefkowitz RJ (2003). Independent beta-arrestin 2 and G protein-mediated pathways for angiotensin II activation of extracellular signal-regulated kinases 1 and 2. Proc Natl Acad Sci U S A 100, 10782–10787. [PubMed: 12949261]

Weisberg SP, McCann D, Desai M, Rosenbaum M, Leibel RL, and Ferrante AW Jr. (2003). Obesity is associated with macrophage accumulation in adipose tissue. J Clin Invest 112, 1796–1808. [PubMed: 14679176]

Wellhauser L, and Belsham DD (2014). Activation of the omega-3 fatty acid receptor GPR120 mediates anti-inflammatory actions in immortalized hypothalamic neurons. J Neuroinflammation 11, 60. [PubMed: 24674717]

Williams-Bey Y, Boularan C, Vural A, Huang NN, Hwang IY, Shan-Shi C, and Kehrl JH (2014). Omega-3 free fatty acids suppress macrophage inflammasome activation by inhibiting NF-kappaB activation and enhancing autophagy. PLoS One 9, e97957. [PubMed: 24911523]

Xu H, Barnes GT, Yang Q, Tan G, Yang D, Chou CJ, Sole J, Nichols A, Ross JS, Tartaglia LA, et al. (2003). Chronic inflammation in fat plays a crucial role in the development of obesity-related insulin resistance. J Clin Invest 112, 1821–1830. [PubMed: 14679177]

Yamada H, Umemoto T, Kakei M, Momomura SI, Kawakami M, Ishikawa SE, and Hara K (2017). Eicosapentaenoic acid shows anti-inflammatory effect via GPR120 in 3T3-L1 adipocytes and attenuates adipose tissue inflammation in diet-induced obese mice. Nutr Metab (Lond) 14, 33. [PubMed: 28503189]

Yki-Jarvinen H (2004). Thiazolidinediones. N Engl J Med 351, 1106–1118. [PubMed: 15356308]

Yu C, Markan K, Temple KA, Deplewski D, Brady MJ, and Cohen RN (2005). The nuclear receptor corepressors NCoR and SMRT decrease peroxisome proliferator-activated receptor gamma transcriptional activity and repress 3T3-L1 adipogenesis. J Biol Chem 280, 13600–13605. [PubMed: 15691842]

CONTEXT AND SIGNIFICANCE

Obesity, a major cause of insulin resistance and Type 2 Diabetes (T2D) in man, is at epidemic levels. Use of pharmacological insulin sensitizers, such as thiazolidinediones (TZDs), which target PPARγ, are highly effective at treating T2D but their clinical utility has been limited by unwanted side effects. Here, Paschoal *et al.* show that combined pharmacological targeting of PPARγ and GPR120 produces additive effects in mouse models of T2D, leading to a greater degree of insulin sensitization than with either drug alone. Importantly, the combined therapy allowed for the use of much lower doses of rosiglitazone, a type of TZD, and, thus, avoiding its unwanted side effects but preserving its overall insulin sensitizing benefit.

HIGHLIGHTS

1. GPR120 is a PPARγ target gene in adipocytes.
2. GPR120 activation blocks the inhibitory phosphorylation of PPARγ at S273
3. GPR120 activation increases the endogenous PPARγ ligand 15d-PGJ2 in adipose tissue.
4. Combined PPARγ and GPR120 agonism potentiates insulin sensitivity in diabetic mice.

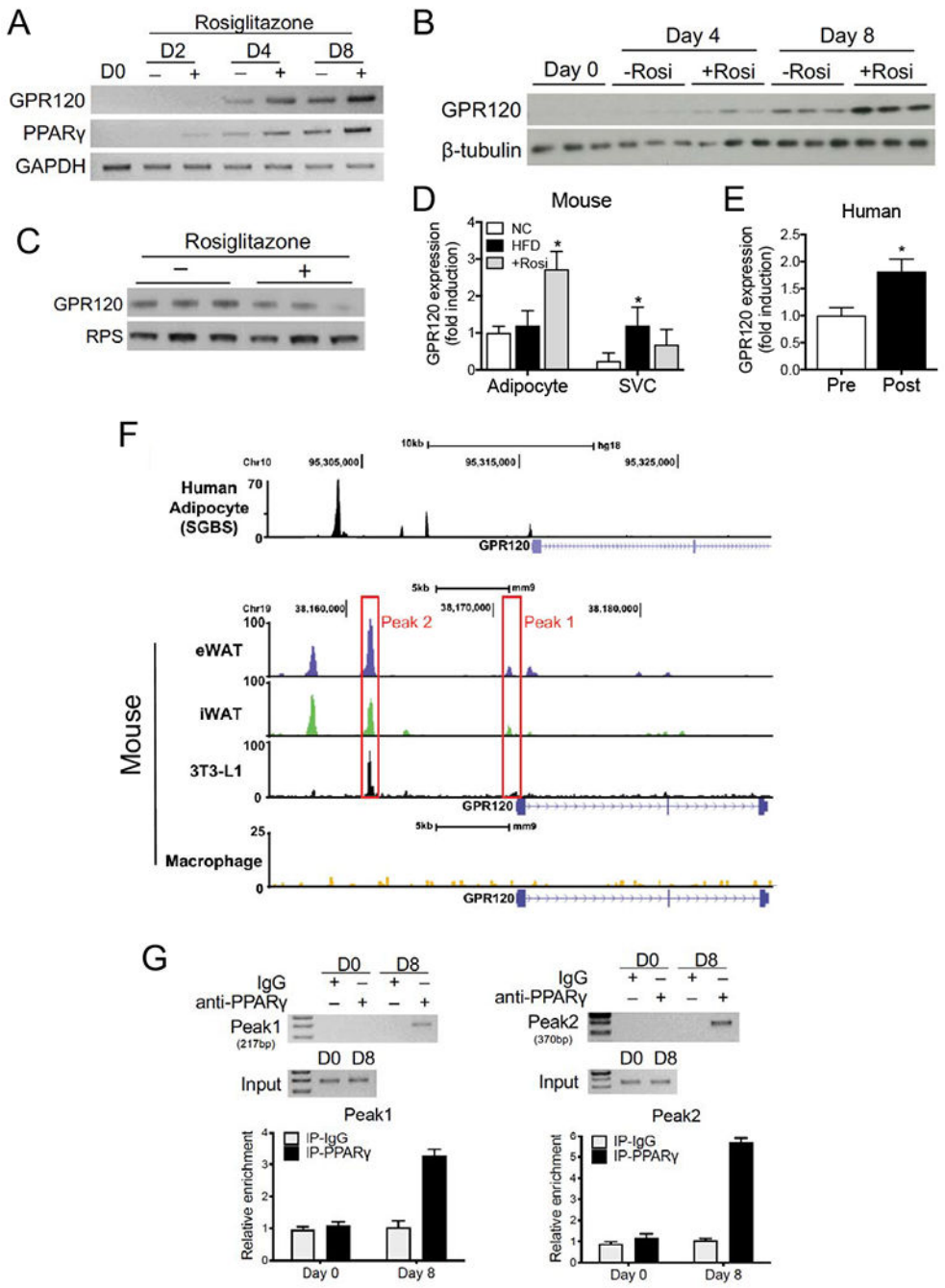

Figure 1. GPR120 expression is regulated by PPARγ in adipocytes.

A, GPR120 mRNA expression as measured by RT-PCR during adipogenic differentiation of 3T3-L1 cells with or without Rosi (1 μM) treatment. PPARγ was included as a positive control for adipocyte differentiation and GAPDH as a loading control. **B,** A representative western blot (n = 3 total western blots) of GPR120 protein expression during primary adipocyte differentiation with or without Rosi (1 μM) treatment. Beta-tubulin was used as a loading control. **C,** GPR120 mRNA expression level in primary macrophages with or without Rosi (1 μM) treatment. Ribosomal protein S3 (RPS) was used as a loading control.

D, Relative GPR120 mRNA expression levels in isolated mouse adipocytes and stromal vascular cells from NC-fed lean, HFD-fed obese, and Rosi- (40 mg/kg for 3 weeks)-treated mice. *, $P < 0.05$ versus NC. **E,** Adipose tissue expression of GPR120 in human subjects after TZD treatment from GEO database, GSE13090 (Sears et al., 2009). *, significant difference between pre- and post-TZD treatment. $P = 0.011$. **F,** Human and mouse ChIP-seq analysis of PPARγ binding peaks in the GPR120 promoter region in adipocytes (mouse and human) and in mouse macrophages. **G,** ChIP-PCR for PPARγ in 3T3-L1 adipocytes on day 0 (D0) and day 8 (D8) of differentiation. IgG was used as a negative control. The PPRE contained in peak 1 (left hand panel) and peak 2 (right hand panel) in the GPR120 promoter were detected by RT-PCR after ChIP. See Table 1 for the primers used for GPR120 promoters. Results are indicated as relative enrichment of immunoprecipitated chromatin compared with IgG. Data and images are representative of at least three independent experiments. All data are expressed as means ± SEM. *, $P < 0.05$ by two-tailed Student's *t*-test. See also Figure S1.

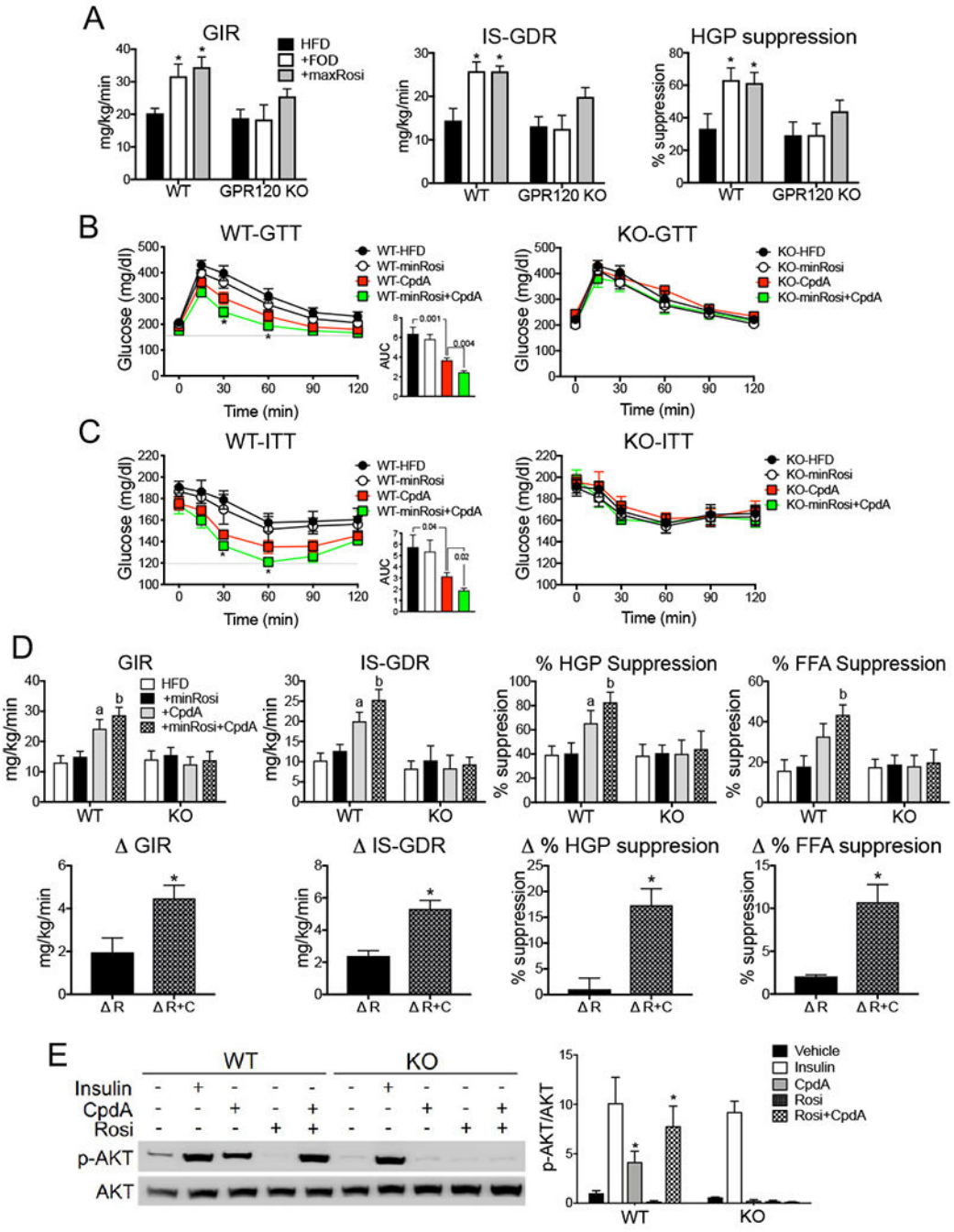

Figure 2. GPR120 activation enhances PPARγ-mediated insulin sensitization.

A, Hyperinsulinemic-euglycemic clamp studies of WT and GPR120 KO mice fed HFD, FOD, or HFD + maximal dose of Rosi (maxRosi; 40 mg/kg). $n = 8$ per group. **B,** GTTs in WT and GPR120 KO mice on HFD, HFD + minimal dose of Rosi (minRosi; 0.8 mg/kg), HFD + CpdA, or HFD + minRosi + CpdA. $n = 12$ per group. *, $P < 0.05$, compared to minRosi. Small bar graph represents the area under the curve (incremental; above basal) for GTTs in WT mice. **C,** ITT in WT and GPR120 KO mice on HFD, HFD + minRosi, HFD + CpdA, or HFD + minRosi + CpdA. $n = 12$ per group. *, $P < 0.05$, compared to minRosi.

Small bar graph represents area under the curve (decremental; above lowest point) of ITT in WT mice. Statistical significance annotation on top of each comparison. **D,** Hyperinsulinemic-euglycemic clamp studies in WT and GPR120 KO mice on HFD, HFD + minRosi, HFD + CpdA, or HFD + minRosi + CpdA. $n = 10$ per group. Glucose infusion rate (GIR), insulin-stimulated glucose disposal rate (IS-GDR), % suppression of hepatic glucose production (HGP), and % suppression of free fatty acid (FFA) levels. *a,* $P < 0.05$ compared to HFD; *b,* $P < 0.05$ compared to minRosi. In the delta calculations underneath each graph, Δ R indicates the difference between HFD and minRosi, while Δ R + C indicates the difference between minRosi + CpdA and CpdA. *, $P < 0.05$ compared to Δ R. **E,** Primary adipocytes from WT and GPR120 KO mice were pretreated with or without Rosi (1 μM) for 24 hr and then subsequently treated with CpdA (10 μM) for 30 min to detect AKT (S473) phosphorylation. Insulin treatment is a positive control. Left panel is a representative image from three independent experiments, and the scanned bar graph (right panel) shows fold induction over basal after normalization for total AKT. *, $P < 0.05$ versus basal. All data are expressed as means ± SEM. (**A, E** two tailed Student's *t*-test; **B, C, D** two-way ANOVA followed by Bonferroni's post hoc test). See also Figures S1 and S2.

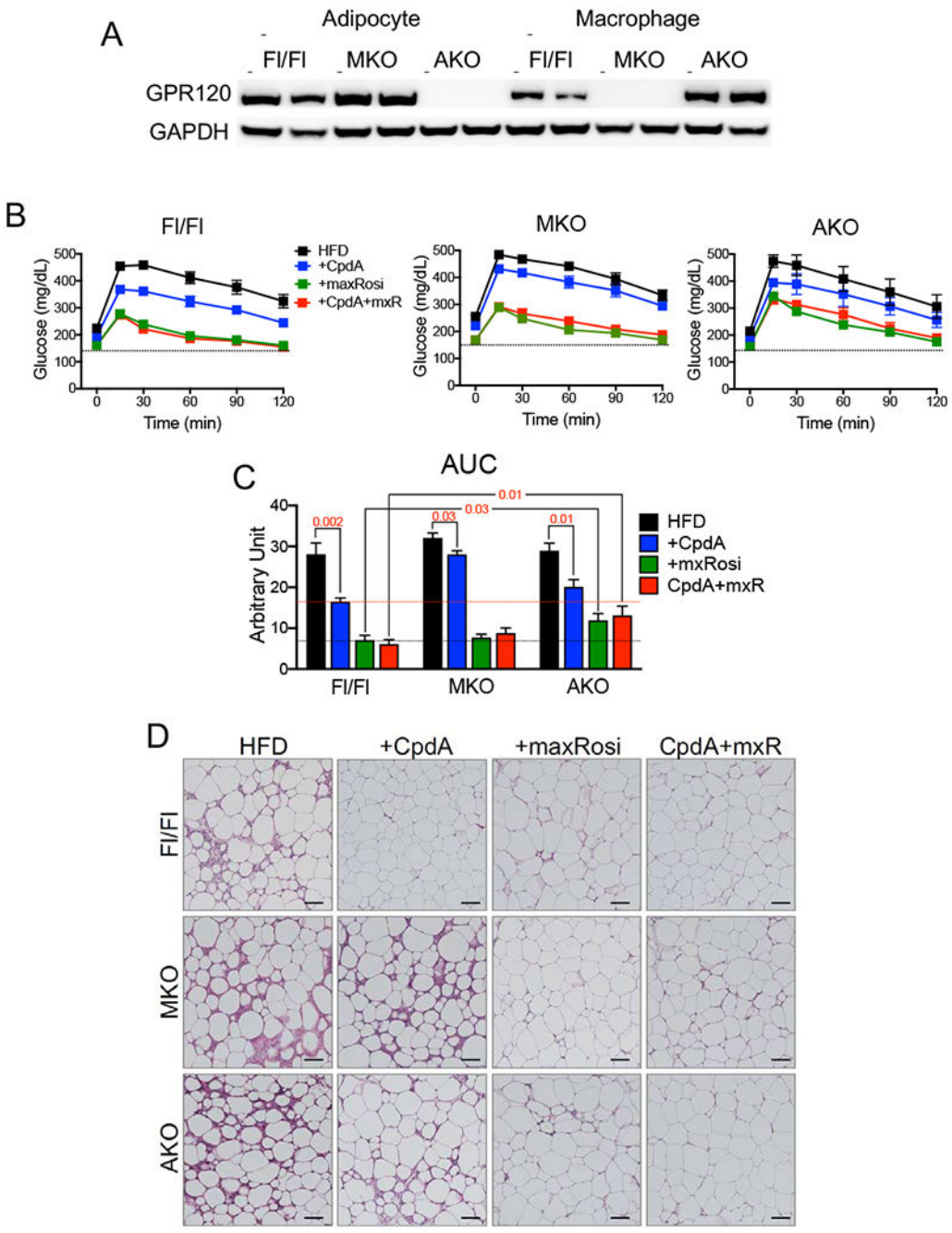

Figure 3. Adipocyte GPR120 enhances positive interacting effects with rosiglitazone.

A. A representative western blot of GPR120 protein expression in adipocytes and macrophages from Fl/Fl, macrophage specific GPR120 KO (MKO), and adipocyte-specific GPR120 KO (AKO) mice to verify tissue-specific deletion. GAPDH as an internal control. Image is a representative image from two independent experiments (n = 4/group). **B.** GTT in Fl/Fl, MKO and AKO mice on HFD, HFD + CpdA (+ CpdA), HFD + maximal dose of Rosi (maxRosi; 40 mg/kg), or HFD + maxRosi + CpdA (CpdA + mxR). n = 8 for Fl/Fl, n = 6 for MKO and AKO. **C.** Incremental area under the curve (AUC) of GTTs. Statistical

significance annotation on top of each comparison. $n = 8$ for Fl/Fl, $n = 6$ for MKO and AKO. **D.** H&E staining of eWAT; scale bar = 100 μm. Data are representative images. $n = 5$ per group. All data are expressed as means ± SEM. (**B, C** two-way ANOVA followed by Bonferroni's post hoc test). See also Figure S3.

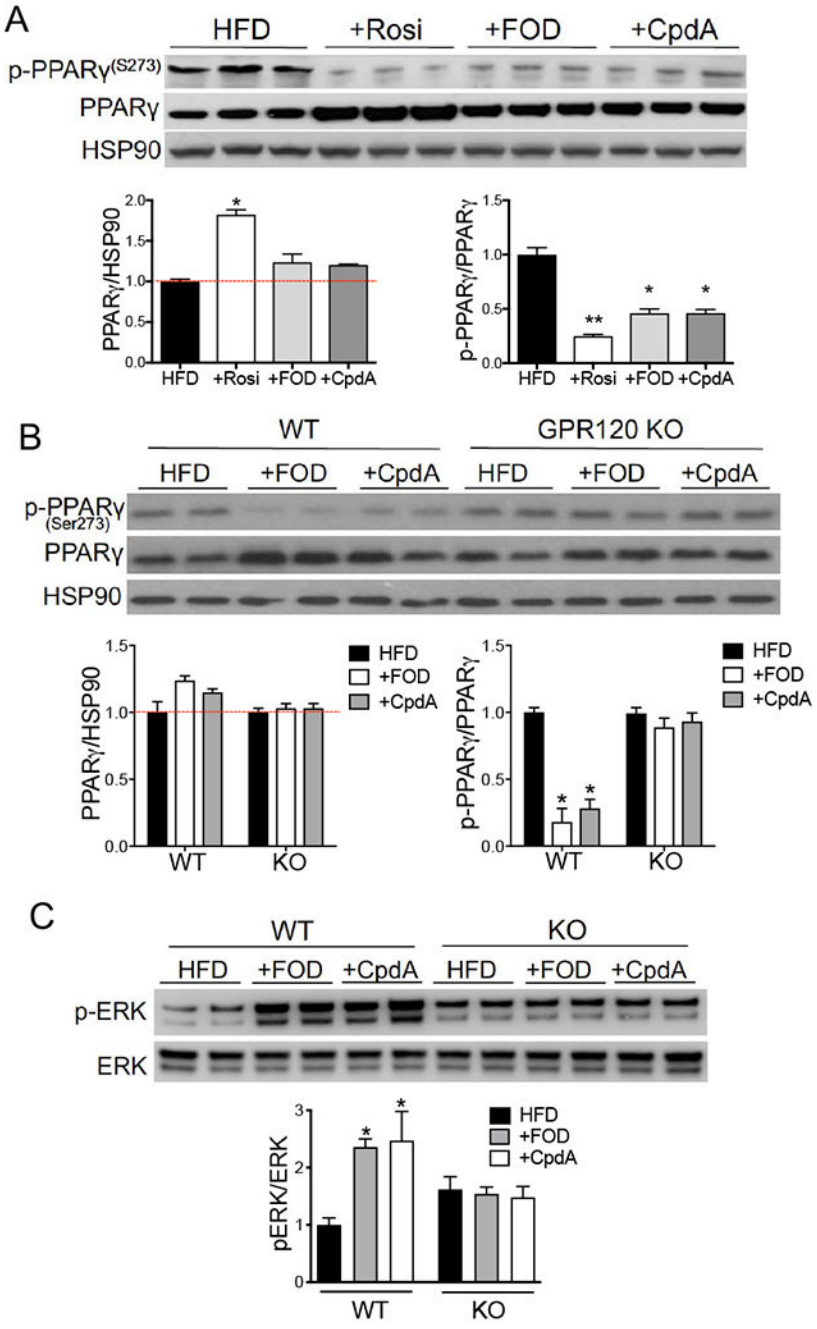

Figure 4. GPR120 stimulation modulates PPARγ S273 phosphorylation.

A, PPARγ S273 phosphorylation level in eWAT from HFD, Rosi, FOD, or CpdA-treated WT mice. **B,** PPARγ S273 phosphorylation level in eWAT from WT and GPR120 KO mice fed HFD, FOD, or CpdA. **C.** Phosphorylation of ERK was measured in adipose tissue from HFD, FOD, or CpdA treated WT and GPR120 KO mice. Data are representative images from at least three independent experiments. The scanned bar graphs are expressed as the mean ± SEM. *, $P < 0.05$; **, $P < 0.05$ versus HFD by two-tailed Student's *t*-test. See also Figures S4 and S5.

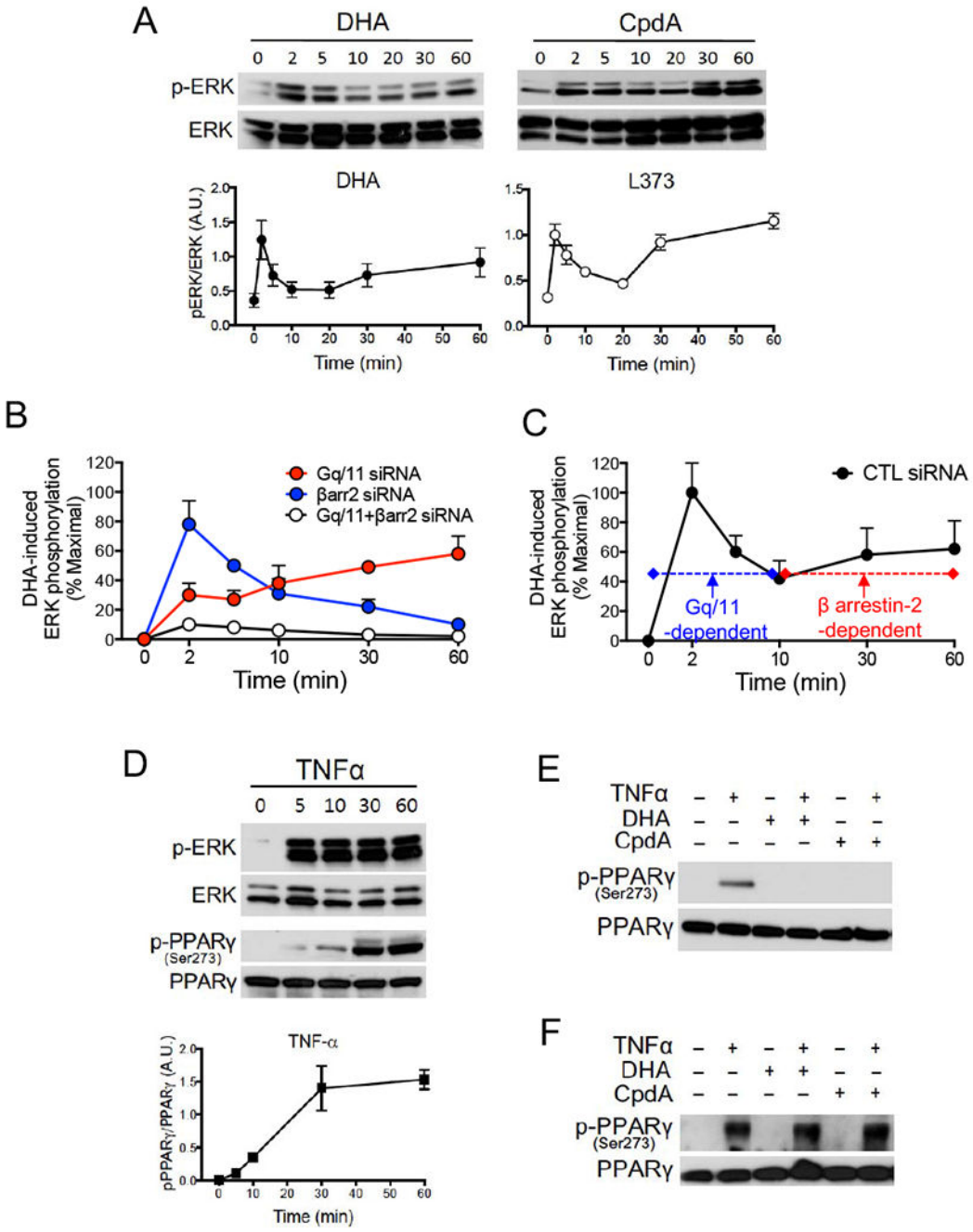

Figure 5. GPR120-mediated biphasic ERK stimulation modulates PPARγ S273 phosphorylation.

A, Time course of ERK phosphorylation induced by DHA (100 μM) and CpdA (10 μM) in HEK293 cells stably expressing GPR120. Each data point in the graphs is expressed as the mean ± SEM and the western blots are representative of at least three independent experiments. **B** and **C,** the kinetics of DHA (100 μM)-induced ERK phosphorylation measured by ELISA in HEK293 cells stably expressing GPR120 and transfected with the indicated siRNA. Data are represented as mean ± SEM from more than three independent experiments. **D,** TNFα (50 ng/ml)-mediated ERK phosphorylation and PPARγ S273

phosphorylation in 3T3-L1 adipocytes as measured by western blotting. The scanned bar graphs are expressed as the mean ± SEM and data are representative images from more than three independent experiments. 3T3-L1 adipocytes were treated with DHA (100 μM) or CpdA (10 μM) for 1 hr **(E)** or 2 min **(F)** prior to TNFα (50 ng/ml, 30 min) treatment and then PPARγ-S273 phosphorylation was measured by western blotting. Data are representative of at least three independent experiments.

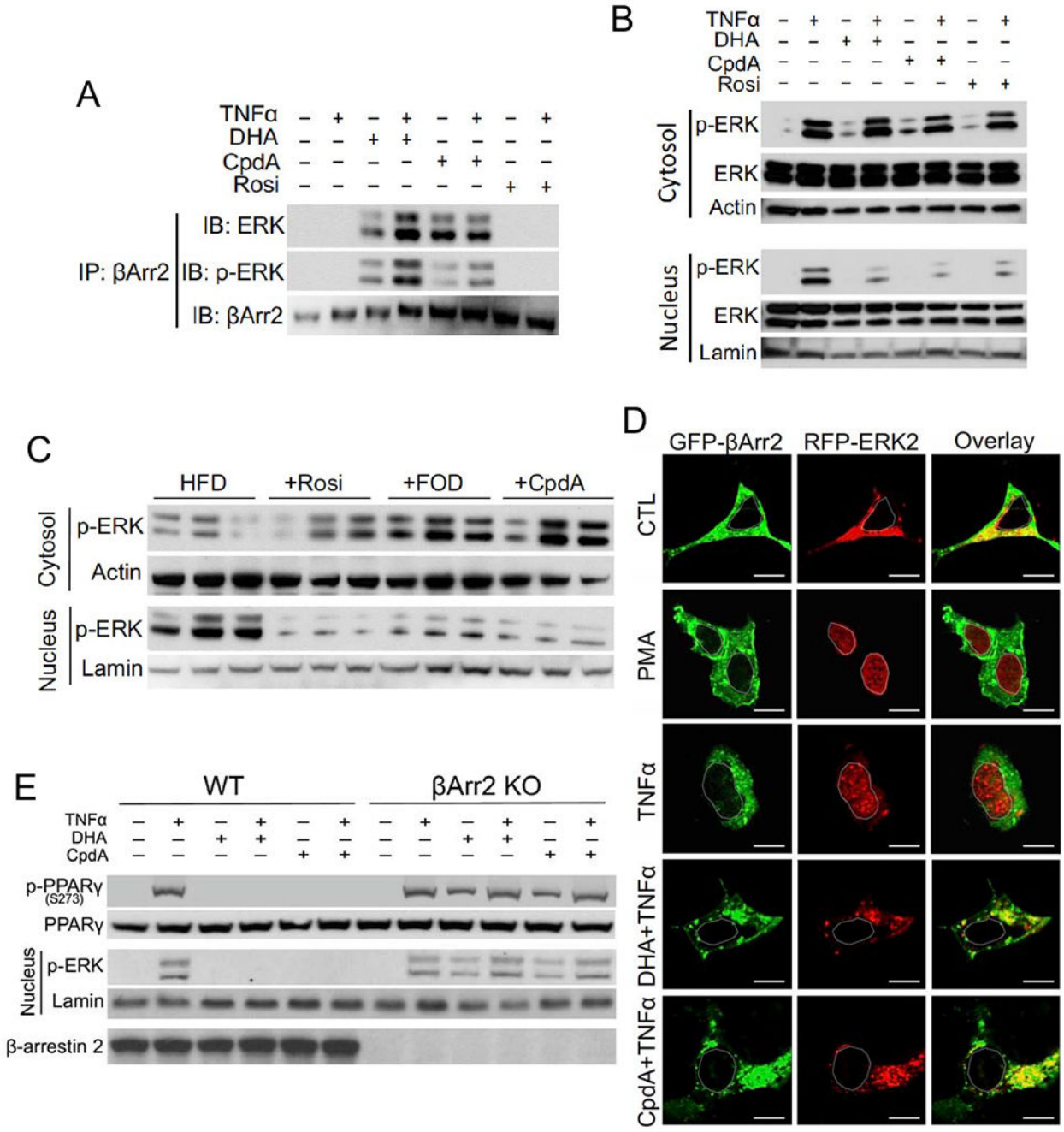

Figure 6. GPR120 stimulation modulates PPARγ phosphorylation via β arrestin-2 association with ERK.

A, Co-immunoprecipitation of β arrestin-2 and ERK in HEK293 cells after GPR120 stimulation. GPR120 stimulation retained phosphorylated ERK in the cytosol and prevented ERK nuclear translocation in **(B)** HEK293 cells stably expressing GPR120 and **(C)** in mouse adipose tissue. Actin, is used as a cytosol marker; Lamin, is used as a nuclear marker. **D,** Fluorescent imaging of HEK293 cells transiently expressing Flag-GPR120, GFP-β arrestin-2, and RFP-ERK2 was performed by confocal microscopy. The nuclear

translocation of ERK induced by 15 min of PMA (1 μM) or TNFα (50 ng/ml) treatment was blocked by 45 min pretreatment with DHA (100 μM) or CpdA (10 μM). Scale bar = 20 μm. White dotted line outlines the nucleus. **E,** GPR120-mediated inhibition of PPARγ-S273 phosphorylation and ERK nuclear translocation was abolished in β arrestin-2 KO primary adipocytes. Data are representative images from more than three independent experiments. See also Figure S6.

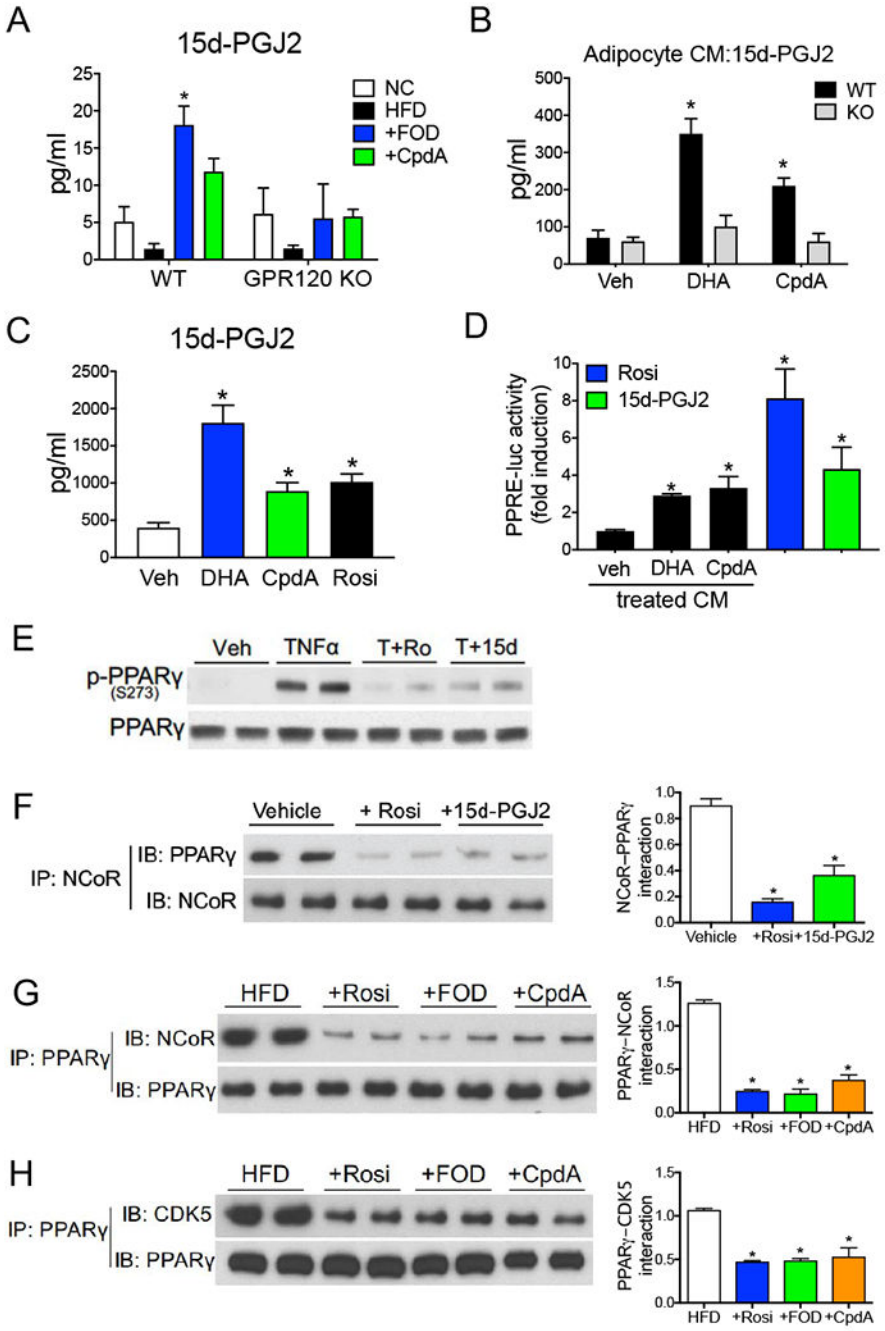

Figure 7. GPR120 stimulation induces the endogenous PPARγ ligand, 15d-PGJ2.

A, Adipose tissue levels of 15d-PGJ2 in WT GPR120 KO mice was measured by Liquid chromatography-mass spectrometry (LC-MS). Data are represented as mean ± SEM. *, $P < 0.05$, compared to HFD by two-tailed Student's *t*-test. $n = 6$ per group. 15d-PGJ2 was measured by ELISA in CM from WT and GPR120 KO primary adipocytes **(B)**, and 3T3-L1 adipocytes **(C)** after treatment with DHA (100 μM), CpdA (10 μM), or Rosi (1 μM) for 24 hr. **D,** 3xPPRE-driven luciferase reporter activity was measured in 3T3-L1 adipocytes treated with CM from **(C)** for 24 hr. Rosi (1 μM) and 15d-PGJ2 (30 μM) for 24 hr were used

as positive controls. Data are represented as mean ± SEM from more than three independent experiments. *, $P < 0.05$, compared to vehicle by two-tailed Student's *t*-test. E, Pretreatment with Rosi (1 μM) and 15d-PGJ2 (30 μM) for 1 hr before TNFα (50 ng/ml) treatment for 30 min inhibited PPARγ S273 phosphorylation in 3T3-L1 adipocytes. **F,** Dismissal of NCoR from PPARγ by Rosi (1 μM) and 15d-PGJ2 (30 μM) treatment for 6 hr was determined by PPARγ co-immunoprecipitation in 3T3-L1 adipocytes. Rosi and GPR120 agonist treatment dismissed binding of PPARγ to NCoR **(G)** and CDK5 **(H)** in mouse adipose tissue. Data are representative images from more than three independent experiments. The scanned bar graphs are expressed as the mean ± SEM. *, $P < 0.05$ versus Vehicle or HFD by two-tailed Student's *t*-test. See also Figure S7.

KEY RESOURCES TABLE

REAGENT or RESOURCE	SOURCE	IDENTIFIER
Antibodies		
Rabbit polyclonal anti-HSP90	Santa Cruz	Cat# sc-382636 RRID: AB_2715499
Rabbit polyclonal anti-PPARγ (for immunoprecipitation)	Santa Cruz	Cat# sc-7196 (H-100) RRID: AB_654710
Mouse monoclonal anti-PPARγ (for western blotting)	Santa Cruz	Cat# sc-7273 (E-8) RRID: AB_628115
Rabbit polyclonal anti-CDK5	Santa Cruz	Cat# sc-173 RRID: AB_631224
Mouse monoclonal anti-pCDK5	Santa Cruz	Cat# sc-377558
Rabbit polyclonal anti-NCoR	Santa Cruz	Cat# sc-8994 (H-303) RRID: AB_2149007
Rabbit polyclonal anti-pS273-PPARγ	Bruce Spiegelman's lab	N/A
Rabbit polyclonal anti-ERK1/2	Cell Signaling	Cat# 9102 RRID: AB_330744
Rabbit polyclonal anti-phospho ERK1/2	Cell Signaling	Cat# 9101 RRID: AB_331646
Rabbit polyclonal anti- β Actin	Cell Signaling	Cat# 4970 RRID: AB_2223172
Rabbit polyclonal anti-Lamin A	Abcam	Cat# ab26300 RRID: AB_775965
Goat polyclonal anti-β arrestin-2	Abcam	Cat# ab31294 RRID: AB_2060265
Mouse monoclonal anti-FLAG (M2)	Sigma-Aldrich	Cat# F1804-200UG RRID: AB_262044
Goat anti-Mouse IgG-Alexa Fluor 546	Invitrogen	Cat# A-11030 RRID: AB_144695
Rabbit polyclonal anti-pS112-PPARγ	Milipore	Cat# 04-816
Plasmids		
Flag-GPR120	(Oh et al., 2010)	N/A
GPR120-pcDNA3	(Oh et al., 2010)	N/A
Gal4-PPARγ	(Li et al., 2011)	N/A
VP16-NCoR	(Li et al., 2011)	N/A
Gal4-CDK5	(Li et al., 2011)	N/A
VP16-PPARγ	(Li et al., 2011)	N/A
3XPPRE-Tk-luc	Addgene	Cat# 1015 RRID: Addgene_1015
β arrestin-2-GFP	Robert Lefkowitz's lab	N/A
RFP-ERK2		N/A
Chemicals, Peptides, and Recombinant Proteins		
Novolin R regular human insulin in ITTs	Novo-Nordisk	Cat# NDC 0169-1833-11
Insulin used in 3T3-L1 adipocyte differentiation	Sigma-Aldrich	Cat# I9278
Dextrose	Hospira, Inc	Cat# 0409-6648-02
^{3}H-deoxyglucose	Perkin Elmer	Cat# NET328001MC
^{3}H-glucose	Perkin Elmer	Cat# NET331C001MC
2-deoxy-D-glucose	Sigma-Aldrich	Cat# D8375
60% high fat diet (HFD)	Research Diets	Cat# D12492
Fish Oil Diet (FOD)	Research Diets	(Oh et al., 2010)

REAGENT or RESOURCE	SOURCE	IDENTIFIER
Lipofectamine RNAiMAX reagent	Thermo Fisher Scientific	Cat# 13778-075
Effectene Transfection Reagent	Qiagen	Cat# 301427
RIPA buffer	Sigma-Aldrich	Cat# R0278-500ML
Collagenase II	Sigma-Aldrich	Cat# C2674
Rosiglitazone	Sigma-Aldrich	Cat# R2408-10MG
Bovine Serum Albumin-low endotoxin, fatty acid free	Sigma-Aldrich	Cat# A8806-5G
cOmplete, Mini, EDTA-free Protease Inhibitor Cocktail	Sigma-Aldrich	Cat# 04693159001
PhosSTOP, phosphatase inhibitor cocktail	Sigma-Aldrich	Cat#4906837001
TRIzol RNA isolation reagent	Thermo Fisher Scientific	Cat# 15596026
SuperScript III	Thermo Fisher Scientific	Cat# 18080051
iTaq SYBR Green supermix	Bio-Rad	Cat# 1725121
RBC lysis buffer	eBioscience	Cat# 00-4333-57
Dynabeads Protein A for immunoprecipitation	Thermo Fisher Scientific	Cat# 10001D
15d-PGJ2	Cayman Chemical	Cat# 18570-1 mg
DHA	Cayman Chemical	Cat# 90310-500 mg
TNFα	R&D Systems	Cat# 510-RT-050
CpdA	Merck & Co., (Oh et al., 2014)	N/A
Critical Commercial Assays		
RNA purification kit	Qiagen	Cat# 74104
Dual luciferase reporter assay system	Promega	Cat# E1910
EpiTect ChIP One-Day Kit	Qiagen	Cat# 334471
Insulin ELISA Kit	ALPCO	Cat# 80-INSHU-E01.1 RRID: AB_2801438
ERK1/2 (Phospho) Multispecies ELISA Kit	Thermo Fisher Scientific	EMS2ERKP
15d-PGJ2 ELISA Kit	Enzo life sciences	ADI-900-023
PGD2 ELISA Kit	Cayman Chemical	Cat# 512031
Deposited Data		
RNA sequencing data	(Oh et al., 2014)	GSE58282
Experimental Models: Cell Lines		
3T3-L1 adipocyte	ATCC	Cat# CL-173 RRID: CVCL_0123
HEK293 cell	ATCC	N/A
HEK293 cell stably expressing GPR120	Pfizer	N/A
Primary macrophage	This paper	N/A
Primary adipocyte	This paper	N/A
Experimental Models: Organisms/Strains		
Mouse: WT C57BL6/J	Jackson Labs.	JAX:000664, RRID: IMSR_JAX:000664
Mouse: GPR120 KO mice and WT littermates	Taconic, (Oh et al., 2010; 2014)	N/A
Mouse: β arrestin-2 KO mice	Jackson Labs.	JAX:011130, RRID: IMSRc_JAX:011130

REAGENT or RESOURCE	SOURCE	IDENTIFIER
ob/ob mice (*Lep*^{ob})	Jackson Labs.	JAX:000632, RRID: IMSR_JAX:000632
Mouse: GPR120 Fl/Fl (C57BL/6-*Ffar4*$^{tm1.1Mrl}$)	Merck & Co.; Taconic	Model 14386
Mouse: Lys M-Cre mice	Chris Glass' lab	N/A
Mouse: Adiponectic-Cre mice	Philipp Scherer's lab	N/A
Mouse: GPR120 MKO (GPR120 Fl/FlxLys M-Cre)	This paper	N/A
Mouse: GPR120 AKO (GPR120 Fl/FlxAdiponectin-Cre)	This paper	N/A
Oligonucleotides		
β arrestin-2 siRNA: 5′-AAGGACCGCAAAGTGTTTGTG	Dharmacon	N/A
Gq/11 siRNA: 5'-GCTGGTGTATCAGAACATC 5'-ACTCACACTTGGTCGATTA	Dharmacon	N/A
Control siRNA: 5'-GGTAGTGCCTGGTAACGTAAA	Dharmacon	N/A
Primers, see Table S1	This paper	N/A
Software and Algorithms		
Image J	NIH	RRID: SCR_003070
Prism	Graphpad	RRID: SCR_002798